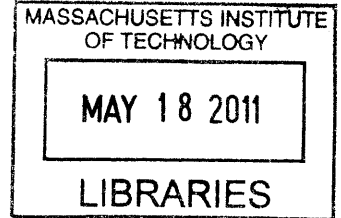


Investigation on Thermal Conductivity and AC

Impedance of Graphite Suspension

by
Jianjian Wang



Submitted to the Department of Mechanical Engineering
in partial fulfillment of the requirements for the degree of

ARCHIVES

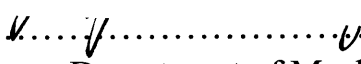
Master of Science in Mechanical Engineering


at the


Massachusetts Institute of Technology

February 2011

©Massachusetts Institute of Technology 2011. All rights reserved.

Author..........
Department of Mechanical Engineering
January 11, 2011

Certified by..........
Gang Chen
Carl Richard Soderberg Professor of Power Engineering

Accepted by..........
David E. Hardt
Chairman, Department of Committee on Graduate Students

Investigation on Thermal Conductivity and AC Impedance of Graphite Suspension

by
Jianjian Wang

Submitted to the Department of Mechanical Engineering
on January 11, 2011, in partial fulfillment of the
requirements for the degree of
Master of Science in Mechanical Engineering

Abstract

Over the past decade, some groups have reported that nanofluids, which are liquids containing suspensions of nanoparticles, have substantially higher thermal conductivity than that of the base fluids. However, the reported high thermal conductivity sometimes cannot be reproduced. Theoretically, potential mechanisms leading to this enhancement are still under scrutiny. In this thesis, we present experimental studies aiming at understanding heat conduction mechanisms in nanofluids. We use graphite flakes as additives and developed methods to prepare stable graphite suspensions. The thermal conductivity enhancement of our suspensions achieved record high thermal conductivity values in different base fluids including water, engine oil, and ethylene glycol. This thesis investigates the effect of graphite flake preparation methods such as microwave and ultrasonic on the thermal conductivity of the suspensions, and found that graphite flakes of tens of nanometer in thickness but tens of microns in size lead to higher thermal conductivity values. To better understand the transport mechanisms, the electrical properties of graphite suspensions are also investigated using AC impedance spectroscopy. The AC impedance spectroscopy leads to insights on how the internal structures of the flake clusters affect heat conduction. Based on the experimental studies, we conclude that the thermal conductivity enhancement in these suspensions is due to percolation heat conduction along graphite flakes.

Thesis Supervisor: Gang Chen

Title: Carl Richard Soderberg Professor of Power Engineering

Acknowledgements

I would like to first and foremost thank my advisor, Professor Gang Chen, who provided me with the great opportunity to study at MIT and work on this exciting project. And he also offered me much help and guidance during my research period.

I especially thank Professor Ruiting Zheng and Professor Jinwei Gao. They taught me a lot of experimental techniques and offered countless help and discussion when I met problems in the research. Professor Ruiting Zheng developed the graphite suspension method and Professor Jinwei Gao conducted initial thermal conductivity studies on the graphite suspensions. I gained a lot from the discussion with Dr. Jaesik Jin. Dr. Tony Feng, an experienced experimentalist on electrochemistry, offered me notable help on the AC impedance experiments. I am really very grateful to Andrew Muto and George Ni, who read my thesis draft and offered very helpful comments. I also want to show my gratitude to Professor Asegun Henry, who gave me quite a lot help during my first year's research at MIT, and express my appreciation to Dr. Shuo Chen, Dr. Sheng Shen, Dr. Tengfei Luo, Yi He and Dr. Qing Hao, who gave me inspirations and hands-on help for my experiments. I am thankful to Professor Shao-Horn Yang who allowed me to use the equipment in her lab, and his student Ethan Crumlin who taught me how to do AC impedance measurements. And I would like to thank all my labmates in the NanoEngineering Group, including some former labmates: Dr. Lu Hu, Dr. Nuo Yang, Yiqun Zhang and Yanjia Zuo.

Finally, I must thank my family and friends for their support, care, and encouragement.

Content

1 Introduction	12
1.1 Background.....	12
1.2 Experimental Investigations of Nanofluids.....	13
1.3 Organization of Thesis	18
2 The Preparation of Graphite Suspensions	20
2.1 Graphite Particles Preparation	22
2.2 Graphite Suspensions Preparation	28
2.3 Summary	31
3 The Thermal Conductivity of Graphite Suspensions	32
3.1 Transient Hotwire Method	32
3.1.1 Measurement Principle	32
3.1.2 Mathematical Derivation.....	33
3.1.3 Experiment Setup.....	35
3.2 Thermal Conductivity Enhancement of Graphite Suspensions with Different Base Fluids.....	40
3.3 The Effect of Microwave Time on the Thermal Conductivity of Graphite Suspensions.....	43
3.4 The Effect of Ultrasonic Time on the Thermal Conductivity of Graphite Suspensions.....	45
3.5 Summary	50

4 Study of Graphite Suspensions Using AC Impedance Spectroscopy	51
.....	
4.1 AC Impedance Theory	52
4.2 AC Impedance Measurement and Analysis of Graphite Suspensions	57
4.2.1 Optical Images of Graphite Particles in Different Base Fluids	57
4.2.2 AC Impedance Spectroscopy and Results Analysis	60
4.3 Summary	71
5 Temperature Regulation of Electrical and Thermal Properties via Phase Transition	73
.....	
5.1 Temperature regulation of electrical and thermal properties	74
5.2 Summary	77
6 Conclusions and Future Work	78
.....	
6.1 Summary and Conclusions.....	78
6.2 Future Work	80

List of Figures

Figure 1-1: Thermal conductivity enhancement of Al_2O_3 in water (Note that some data were measured at different temperatures or using different diameter of nanoparticles). Figure is redrawn using data from Ref. [14-19].	14
Figure 1-2: Effect of particle material on the thermal conductivity enhancement of nanofluids (base fluids: ethylene glycol). Figure is redrawn using data from Ref. [12, 16, 20, 21].	15
Figure 1-3: Effect of base fluid materials on the thermal conductivity enhancement of Al_2O_3 nanofluids. Figure is redrawn using data from Ref. [14, 16].	16
Figure 1-4: Effect of particle shape on the thermal conductivity enhancement of nanofluids. Figure is redrawn using data from Ref. [16].	17
Figure 2-1: Enhanced thermal conductivity with/without surfactant at room temperature for both CuO and alumina nanofluids. Figure is redrawn using data from Ref. [47].	22
Figure 2-2: Expanded graphite particles after microwave expansion: (a) optical image, (b) SEM image.	24
Figure 2-3: The original graphite flakes without any treatment are hydrophobic to water but hydrophilic to oil. After microwave expansion, they become much less hydrophobic to water and less hydrophilic to oil. This behavior is because the microwave expansion treatment brings new functional groups to the surfaces of graphite flakes.	25
Figure 2-4: Graphite particles zeta potential in DI water as a function of microwave time. The longer microwave time is, the smaller the absolute value of zeta potential is.	27
Figure 2-5: Graphite particles zeta potential in ethylene glycol as a function of microwave time. The longer microwave time is, the smaller the absolute value of zeta potential is.	27
Figure 2-6: Graphite particles zeta potential in hexadecane as a function of microwave time. The longer microwave time is, the smaller the absolute value of zeta potential is.	28
Figure 2-7: Ultrasonic setup. Sometimes when long ultrasonic time is needed, it is better to put the small suspension sample container into a big container which contains cooling water so that the ultrasonic probe and the suspension sample will not be overheated.	29

Figure 2-8: SEM image of graphite flakes after ultrasonic preparation.....	30
Figure 2-9: TEM image of graphite flakes after ultrasonic preparation.....	30
Figure 2-10: Optical images of graphite suspensions with different base fluids: PAO, Ethylene Glycol, and DI water. The small insets are pictures of graphite suspensions samples which were taken three months after the preparation.....	31
Figure 3-1: Three heat conduction regions: bare metallic wire, electrical insulating layer, and surrounding medium.	33
Figure 3-2: Thermal conductivity measurement cell.	36
Figure 3-3: Wheatstone bridge circuit for transient hotwire equipment.	37
Figure 3-4: Transient hotwire measurement setup.	39
Figure 3-5: The thermal conductivity of graphite suspensions at different volume fraction in three kinds of base fluids.	41
Figure 3-6: The thermal conductivity enhancement of graphite suspensions at different volume fraction in three kinds of base fluids.....	42
Figure 3-7: The thermal conductivity enhancement of three kinds of graphite suspensions as a function of volume fraction.....	43
Figure 3-8: Thermal conductivity of PAO/graphite suspensions vs. microwave time.....	44
Figure 3-9: Thermal conductivity enhancement as a function of sonication time.	46
Figure 3-10: SEM image of graphite flakes after sonicating 20 minutes. The average graphite flake diameter is about $7.3 \mu m$ based on the statistics from SEM image.	46
Figure 3-11: SEM image of graphite flakes after sonicating 60 minutes. The average graphite flake diameter is about $4.1 \mu m$ based on the statistics from SEM image.	47
Figure 3-12: SEM image of graphite flakes after sonicating 120 minutes. The average graphite flake diameter is about $1.9 \mu m$ based on the statistics from SEM image.	47
Figure 3-13: Several sets of data on the thermal conductivity enhancement of ethylene glycol based graphite suspensions. These sets of suspension samples were prepared by the same method but using different ultrasonic times. Generally, higher volume fraction samples were prepared using longer ultrasonic time; lower volume fraction samples	

were prepared using shorter ultrasonic time. For the same volume fraction samples, we adjusted the ultrasonic time to control the thermal conductivity to be a little higher or lower. 48

Figure 3-14: Comparison of the thermal conductivity of ethylene glycol based graphite suspensions which are prepared using different ultrasonic time. For the blue curve, the ultrasonic time of each sample is about 25 minutes. For the black curve, the ultrasonic time of each sample is about 30 minutes. For the red curve, the ultrasonic time of each sample is different. Obviously the ultrasonic time strongly affects the thermal conductivity of graphite suspensions. And the longer ultrasonic time is, the smaller thermal conductivity will be..... 49

Figure 4-1: A typical electrical circuit – parallel of a resistor R and a capacitor C.....53

Figure 4-2: The “Nyquist Plot” of the electrical circuit Fig. 4-1. 54

Figure 4-3: Optical image of graphite particles in PAO (vol. fraction: 0.1%) 58

Figure 4-4: Optical image of graphite particles in ethylene glycol (vol. fraction: 0.1%) 58

Figure 4-5: Optical image of graphite particles in DI water (vol. fraction: 0.1%)..... 59

Figure 4-8: An example of AC impedance measurement curve and fitting curve of ethylene glycol based graphite suspension with the volume fraction 0.14%. The fitting curve is based on the model shown in Fig. 4-9..... 62

Figure 4-9: The equivalent circuit we used to model the impedance behavior of graphite suspensions. It contains three RC parallel units [51]. The first RC unit denotes for the cluster internal response, where R_{ci} is the cluster internal resistance and C_{ci} is the cluster internal capacitance. The second RC unit denotes for the cluster-cluster response, where R_{cc} is the cluster-cluster resistance and C_{cc} is the cluster-cluster capacitance. The third RC unit denotes for the electrode response, where R_e is the solution resistance and C_e is the double layer capacitance at the electrode. 62

Figure 4-10: Cluster-cluster conductance & capacitance and cluster internal conductance & capacitance as a function of graphite volume fraction in ethylene glycol. 63

Figure 4-11: Thermal conductivity enhancement of ethylene glycol based graphite suspensions. The

samples used in this figure correspond to the samples in Fig. 4-10.	64
Figure 4-13: The relation between logarithm of cluster-cluster conductance K and logarithm of volume fraction ϕ in the percolation region.	66
Figure 4-14: Cluster-cluster conductance & capacitance and cluster internal conductance & capacitance as a function of graphite volume fraction. Samples are prepared using shorter ultrasonic time compared with the samples of Fig. 4-10.	68
Figure 4-15: Thermal conductivity enhancement of ethylene glycol based graphite suspensions. Samples are prepared using shorter ultrasonic time compared with the samples of Fig. 4-11. The samples used in this figure are corresponding to the samples in Fig. 4-14.	69
Figure 4-16: The relation between logarithm of cluster-cluster conductance K and logarithm of volume fraction ϕ in the percolation region. The samples used in this figure correspond to the samples in Fig. 4-14.	70
Figure 5-1: Electrical conductivity contrast after different cycles. Blue lines indicate the electrical conductivity of 0.8% hexadecane based graphite nanocomposites in the course of freezing, while red lines indicate that in the course of melting.	75
Figure 5-2: Thermal conductivity contrast after different cycles. Blue lines indicate the thermal conductivity of 0.8% hexadecane based graphite nanocomposites at 3 °C during different cycles, while red lines indicate that at 25 °C during different cycles.	76
Figure 5-3: Conceptual illustration of the contact area variation between graphite flakes submerged in hexadecane in the course of hexadecane freezing and remelting. The anisotropic growth the hexadecane crystals will generate pressure on the surface of graphite flakes, which increases the contact area and reduces the flake separation. When the frozen hexadecane remelts, the pressure is released and the contact area decreases again.	77

Chapter 1

Introduction

1.1 Background

Thermal conductivity of heat transfer fluids play an important role in the industry of heat-exchange equipments. Researchers [1] have tried to add micro or large-sized particles into the fluids to increase the thermal conductivity, as the solid particles usually have much higher thermal conductivity than the liquid. The thermal conductivity of these suspensions can be predicted by the effective medium or mean-field theory of Maxwell [2]:

$$\frac{k}{k_f} = \frac{1+2\beta\varphi}{1-\beta\varphi} \quad (1.1)$$

where k is the thermal conductivity of the suspension, k_f is the thermal conductivity of base fluid, φ is the particle volume fraction, $\beta = (k_p - k_f) / (k_p + 2k_f)$ and k_p is the thermal conductivity of particles. If the interfacial thermal resistance between the particles and the base fluid is considered, Maxwell effective medium theory still holds true, provided that one makes the substitution $k_f \rightarrow k_f(1 + 2R_b k_p / d)$ on the right hand side of Eq. (1.1), where R_b is the interfacial thermal resistance and d is the particle diameter [3]. However, due to the large size and high density of the particles, there is no way to prevent the settlement of particles out of the suspension. There are also some other drawbacks that limit its application [4-6]. The particles are likely to: 1) clog the pipes when the particles settle down, 2) abrade the inner surface of pipes due to the higher inertia of the large particles, and 3) increase the pressure drop along the pipe and thus increase the cost of the power supply.

Masuda et al. [7] were the first to conduct experiments to show that the thermal conductivity and viscosity of liquids alter when it contains ultrafine particles (13nm). However, the term nanofluids, which are suspensions of nanoparticles in a base fluid, was proposed in 1995 by Choi [8-9] who worked at Argonne National Lab in the United States. Since Choi's work, some groups have observed that nanofluids have superior heat transfer performance (such as enhanced thermal conductivity, convective/boiling heat transfer coefficient) compared to the conventional heat transfer fluids, as well as fluids containing micro-sized particles. Due to the much smaller particle size, the settlement possibility is significantly reduced; therefore nanofluids could be much more stable and have the potential for practical application. Consequently these advantages of nanofluids have led both industry and universities to launch research and development efforts. For the thermal conductivity experiments of nanofluids, Choi and some groups [10-11] observed large thermal conductivity enhancements beyond the effective medium theory predictions. However, other groups could not repeat these experiments results, and mechanisms for the extraordinary thermal conductivity enhancements of nanofluids, if exists, are still under debate. Investigation on the heat conduction mechanisms is the main goal of this thesis.

1.2 Experimental Investigations of Nanofluids

Earlier researchers found that even low particle volume fractions nanofluids can enhance the thermal conductivity significantly compared to the base fluids. Eastman and Choi [12] reported that the copper (10 nm) nanofluids with ethylene glycol as the base fluid can achieve 40% thermal conductivity enhancement at the volume fraction 0.3%. Jana et al. [13] reported 74% enhancement using the same kind of nanofluids at the same volume fraction. Liu et al. observed 23.8% thermal conductivity enhancement for copper nanofluids at the volume fraction 0.1%. Generally, many parameters can affect the

thermal conductivity enhancement of nanofluids, such as particle volume fraction, particle material, base fluid, temperature, pH, and nanofluids preparation method which affects the particle size and shape [14].

Figure 1-1 shows the experimental data of nanofluids thermal conductivity from different research group. The nanoparticles used in these experiments are Al_2O_3 (spherical), and the base fluid is water. We can see that thermal conductivity of nanofluids generally will increase as the particle volume fraction increases. Das et al. [15] investigated the temperature effect on the thermal conductivity enhancement. Results show that as the temperature increase, the thermal conductivity enhancement of Al_2O_3 /water nanofluids also increases. Xie et al. [16], Wang et al. [17], and Lee et al. [18] investigated particle size effect on the enhancement. However, the trends shown in Fig. 1-1 are not monotonic (thermal conductivity ratio: 60nm > 28nm > 38nm).

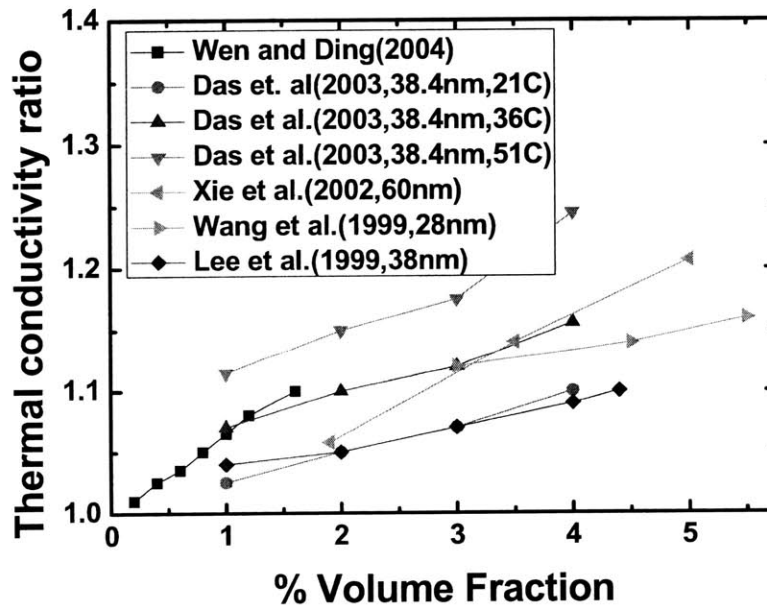


Figure 1-1: Thermal conductivity enhancement of Al_2O_3 in water (Note that some data were measured at different temperatures or using different diameter of nanoparticles). Figure is redrawn using data from Ref. [14-19].

Figure 1-2 shows the effect of particle material on the thermal conductivity enhancement of nanofluids. The base fluid used in these experiments is ethylene glycol. It can be seen that the thermal conductivity ratio increases much faster for metallic particles than metallic oxide particles [14].

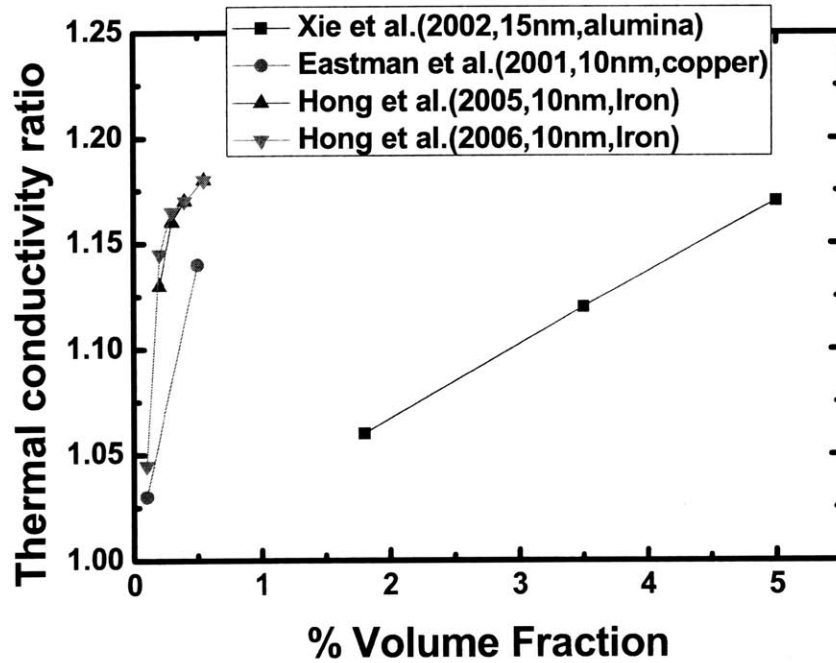


Figure 1-2: Effect of particle material on the thermal conductivity enhancement of nanofluids (base fluids: ethylene glycol). Figure is redrawn using data from Ref. [12, 16, 20, 21].

Figure 1-3 shows the effect of base fluid materials on the thermal conductivity enhancement of Al_2O_3 nanofluids. The thermal conductivities of water, ethylene glycol and pump oil are 0.6 W/mK , 0.25 W/mK and 0.14 W/mK . The experimental results indicate that the thermal conductivity enhancement is larger for poor heat transfer (low thermal conductivity) fluids.

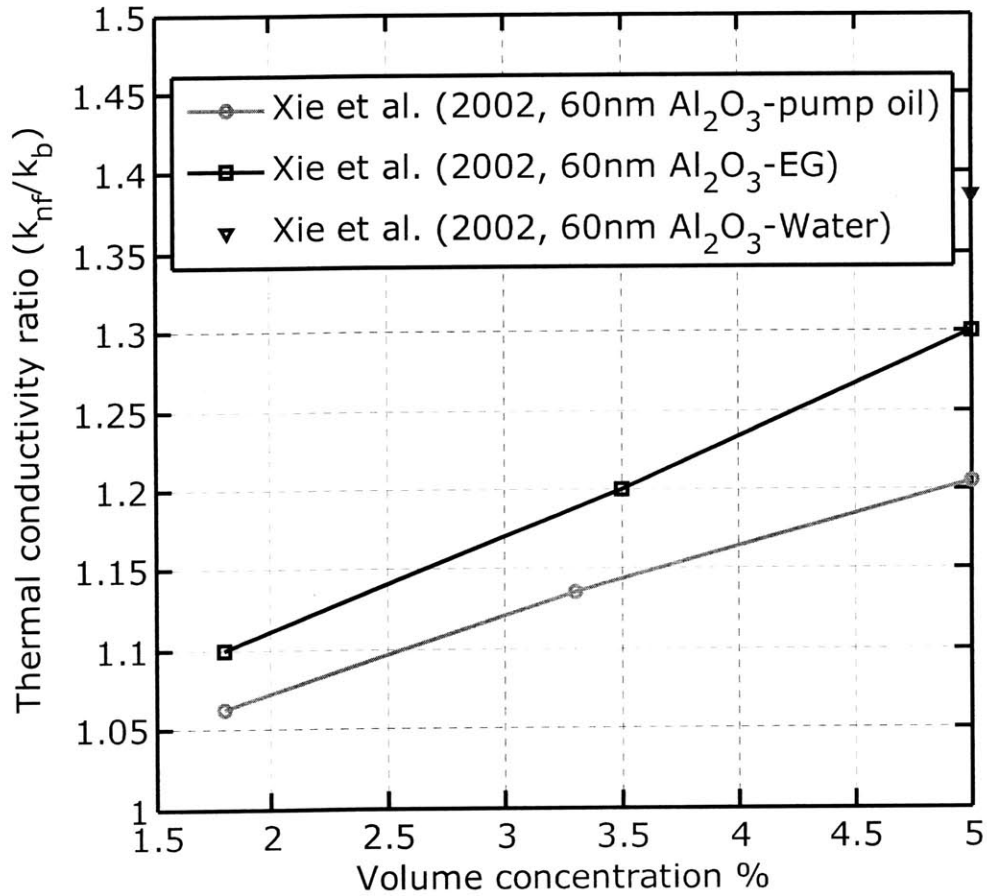


Figure 1-3: Effect of base fluid materials on the thermal conductivity enhancement of Al_2O_3 nanofluids. Figure is redrawn using data from Ref. [14, 16].

Figure 1-4 shows the effect of particle shape on the thermal conductivity enhancement of SiC nanofluids. Different from the factors of temperature, particle volume fraction, particle materials and base fluid materials, which are parameters that are much easier to control; particle shape and particle size are determined by the preparation method, which are much more difficult to control. From the figure we can see that the nanofluids with cylindrical particles have higher thermal conductivity enhancement than that of spherical particles [14].

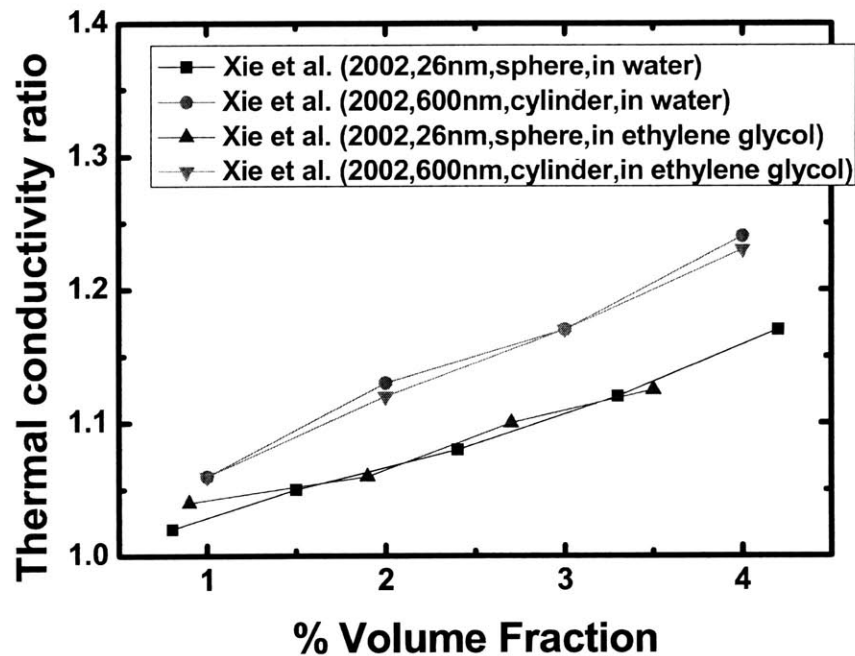


Figure 1-4: Effect of particle shape on the thermal conductivity enhancement of nanofluids. Figure is redrawn using data from Ref. [16].

Here we should mention that it is not completely believed by all the researchers that nanofluids could significantly increase the thermal conductivity of the base fluid. For example, Putnam et al. [22] measured the thermal conductivity of gold (4nm) nanofluids, and observed only $1.3\% \pm 0.8\%$ enhancement, which obviously contradicted with the results from Patel et al. [23]. In a recent round-robin study of several different nanofluids with 33 groups participated, no extraordinary thermal conductivity enhancement beyond the prediction of effective medium theory was observed [24-25]. Therefore there are still quite a lot of debate since nanofluids was proposed by Choi 15 years ago, even on whether the experimental results are believable or not.

The heat conduction mechanisms of nanofluids are also of great interest. Different models have been proposed to explain different experimental data, such as Brownian motion of nanoparticles [26-27], molecular-level layering of the liquid at the

liquid/nanoparticle interface [28-33], clustering of nanoparticles [34-35], the nature of heat transport in the nanoparticles [34, 36], and thermophoresis (ordered movements of nanoparticles due to the temperature gradient) [37-38].

Gao et al. [39] investigated the heat conduction mechanisms of nanofluids by freezing the alumina nanofluids. After freezing the Brownian motion effect in the composite is significantly reduced. They observed that the thermal conductivity enhancements are even higher in the solid state compared with that in the liquid state when the liquid forms crystals upon solidification. Transmission electron microscope (TEM) images indicate that there are many clusters within the composite. When the composite is frozen, clusters are likely to form a percolation network structure if the host material is crystal in the solid state. Based on the experiments, they concluded that nanoparticles clustering should be the key contributor for the enhanced thermal conductivity of nanofluids because in this case heat prefers to conduct along the clusters that are composed of high thermal conductivity nanoparticles. Inspired by this paper, we choose to investigate the heat conduction mechanisms of graphite suspension. This is based on two facts, first graphite particles are flake shape which is much easier to form clusters within the suspension; second graphite has very high in-plane thermal conductivity. It is envisioned that the thermal boundary resistance between graphite flakes is likely to be bad for heat conduction along the clusters. To reduce the thermal boundary resistance, graphite flakes can be made into larger particles as long as stable suspensions can be formed.

1.3 Organization of Thesis

The thesis aims at investigating the heat conduction mechanisms of graphite suspensions, and is organized as follows. Chapter 1 discusses the background information on the nanofluids research area. Chapter 2 introduces a method for the preparation of graphite suspensions which can be stable in both ethylene glycol/PAO and water. Chapter 3

presents the thermal conductivity measurement principle, discusses the experimental results on the thermal conductivity enhancement of graphite suspensions, and investigates many factors that might affect the thermal conductivity of our suspensions. Chapter 4 investigates the heat conduction mechanisms of graphite suspensions using AC impedance spectroscopy, and analyzes the resistance and capacitance effects within the suspensions. These experiments shed light on the internal structures of the graphite suspensions. Chapter 5 discusses the thermal and electrical regulation of graphite suspensions via phase transition. Chapter 6 summarizes the thesis and discusses future directions.

Chapter 2

The Preparation of Graphite Suspensions

The preparation of nanofluids (or suspension) is the first step in experimental investigation. There are mainly two techniques to produce the nanofluids: the two-step technique and the single-step technique. The two-step technique is mainly used in the synthesis of nanofluids using the available nanoparticles [40]. In this method, nanoparticles is first produced by using a physical or chemical synthesis method, and then dispersed into the base fluid. For example, Eastman et al. [41], Lee et al. [18], and Wang et al. [17] used the two-step method to prepare Al_2O_3 nanofluids. The single-step technique produces and disperses the nanoparticles into the base fluid simultaneously [14]. One single-step direct evaporation approach was developed by Akoh et al. [42] and is called VEROS (Vacuum Evaporation onto a Running Oil Substrate) technique. Later a modified VEROS technique was developed by Wagener et al. [43]. They used high pressure magnetron sputtering for the preparation of suspension with metal nanoparticles. Eastaman et al. [41] developed another modified VEROS technique, in which Cu vapor is directly condensed into nanoparticles by contact with a flowing low-vapor-pressure liquid such as ethylene glycol. The single-step technique is usually used to produce nanofluids containing metallic nanoparticles. The two-step technique is usually employed to produce nanofluids which contain oxide nanoparticles or carbon nanotubes.

Here we want to mention that the greatest challenge of making nanofluids is the stability. There are two mechanisms about the stability of colloidal systems. One is electrostatic stabilization mechanism, the other one is polymeric stabilization mechanism [44]. The most classical theory on the electrostatic stabilization

mechanisms is DLVO theory [45, 46], which was developed by Derjaguin, Verwey, Landau and Overbeek in 1940s. It suggests that the stability of colloidal system is determined by the sum of the van der Waals force and electrostatic force between particles. The repulsive electrostatic force (if this is the net effect) will prevent the particles adhering together to stabilize the colloidal system. The polymeric stabilization of colloidal system [44] involves the polymeric molecules (surfactant) added into the colloids to prevent the particles adhering to each other. Essentially the polymeric molecules create a repulsive force counterbalancing the attractive van der Waals force between particles to stabilize the colloidal system. Phenomenologically, when the nanoparticles are hydrophobic to the base fluids, it is very hard to prepare stable nanofluids. In this case, surfactant is usually used to wrap the nanoparticles (polymeric stabilization mechanism) and thus to improve the nanoparticles' ability to disperse. However, the existence of surfactant increases the interfacial resistance between the nanoparticles and base fluids, therefore reduces the thermal conductivity enhancement of nanofluids if the heat conduction is primary along the nanoparticles. Figure 2-1 shows that the addition of surfactant substantially reduces the thermal conductivity by more than 30% compared with that of nanofluids without surfactant [47].

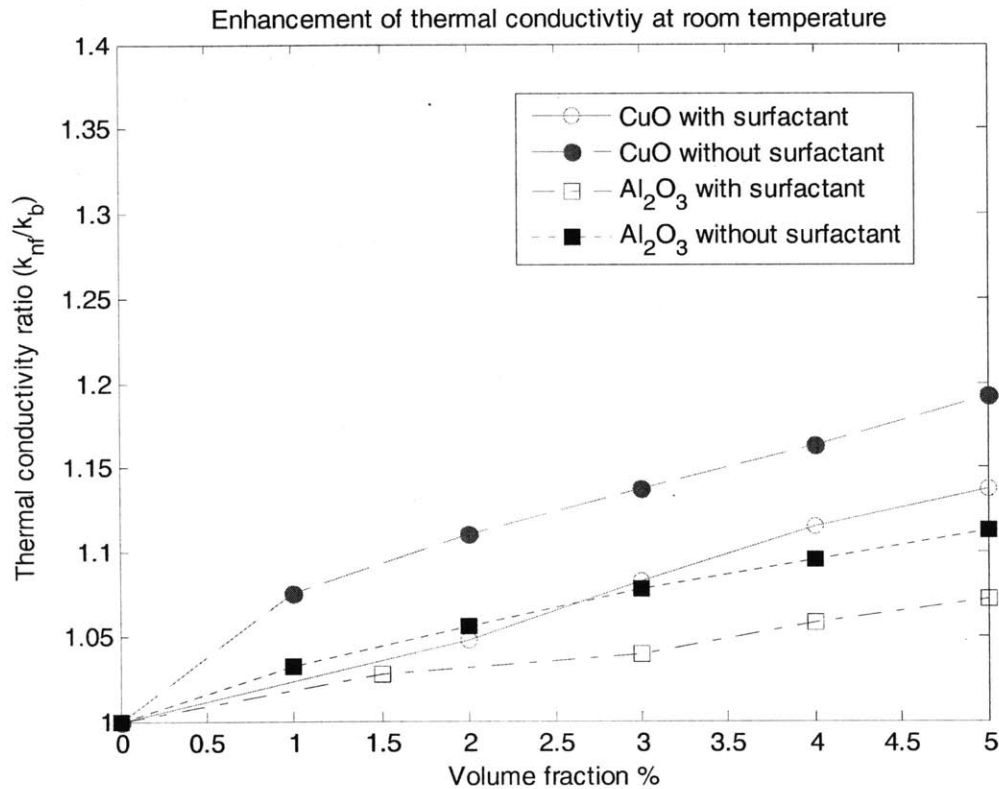


Figure 2-1: Enhanced thermal conductivity with/without surfactant at room temperature for both CuO and alumina nanofluids. Figure is redrawn using data from Ref. [47].

The preparation of our graphite suspensions is a two-step method. It follows sulfuric acid intercalation and microwave expansion processes to get the graphite particles, and then an ultrasonic process to make the graphite suspensions. No surfactant is needed to get the stable suspensions in our preparation process. We describe the preparation processes in this chapter.

2.1 Graphite Particles Preparation

Usually nature graphite particles are large-sized and too thick, which cannot be directly mixed with base fluid as the particles tend to agglomerate and settle out very quickly. To avoid this happening, we need to do some treatment to the nature graphite particles. The treatment not only enables us to prepared stable graphite suspensions,

but also endows the particles with the ability to form percolation structures within the suspension at even low volume fraction. Generally we use chemical intercalation [48-53] and microwave expansion to obtain exfoliated graphite flakes with desired functional groups on the surface, and followed by an ultrasonic process to further reduce the graphite flake size and produce the graphite suspension samples.

The chemical intercalation is a process of the insertion of atomic or molecular layer of a different chemical species between layers in a graphite host material [54]. The microwave expansion is essentially not only a rapid heating process which creates pressure between graphite layers and thus significantly expands the interlayer spacing, but also an oxidation process which brings new functional groups on the surface of graphite particles. In our case, 85ml H_2SO_4 (96%) and 15ml hydrogen peroxide (30%) were mixed as an oxidative agent for the intercalation. For the intercalation process, 2.2 g of nature graphite was reacted with 100ml oxidative agent at room temperature for 60 min. The slurries were rinsed with distilled water to remove residual salts and acids, followed by filtering and baking on a hotplate at 110 °C for 24 hour. The expanded graphite was obtained by rapid expansion of as-prepared graphite intercalation compounds (contained in a 250ml plastic beaker) in a commercial microwave oven (SANYO 1100-Watt) for 30 sec. This rapid heating process would greatly increase the volume of graphite particles (about 100~1000 times volume increment). Figure 2-2 shows the optical image and SEM image of graphite after microwave expansion.

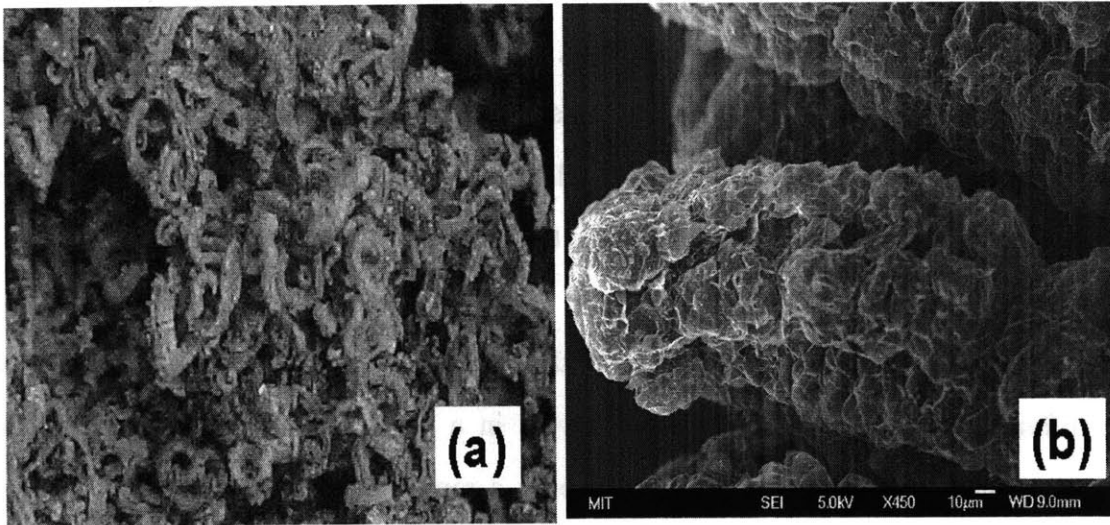


Figure 2-2: Expanded graphite particles after microwave expansion: (a) optical image, (b) SEM image.

In our experiments, we choose three base fluids: de-ionized water (DI water), ethylene glycol, and Poly-alpha-olefin (PAO). Nature graphite is hydrophilic to ethylene glycol and PAO but hydrophobic to DI water. However, the microwave expansion process could change the graphite particle's hydrophilicity/hydrophobicity to some extent (see Fig. 2-2). X-ray photoelectron spectroscopy (XPS) of graphite flakes tells us [53] that the microwave expansion brings new functional groups, such as C=C, C=O, C-OH, and O=C-OH, to the surface of graphite particles and thus changes the charge distribution on the surface of graphite particles. The interactions between hydrophilic functional groups from different particles supply an extra short range repulsive force [55] and thus prevent the adhesion of particles. This is the reason why the graphite particles suspension stability is enhanced.

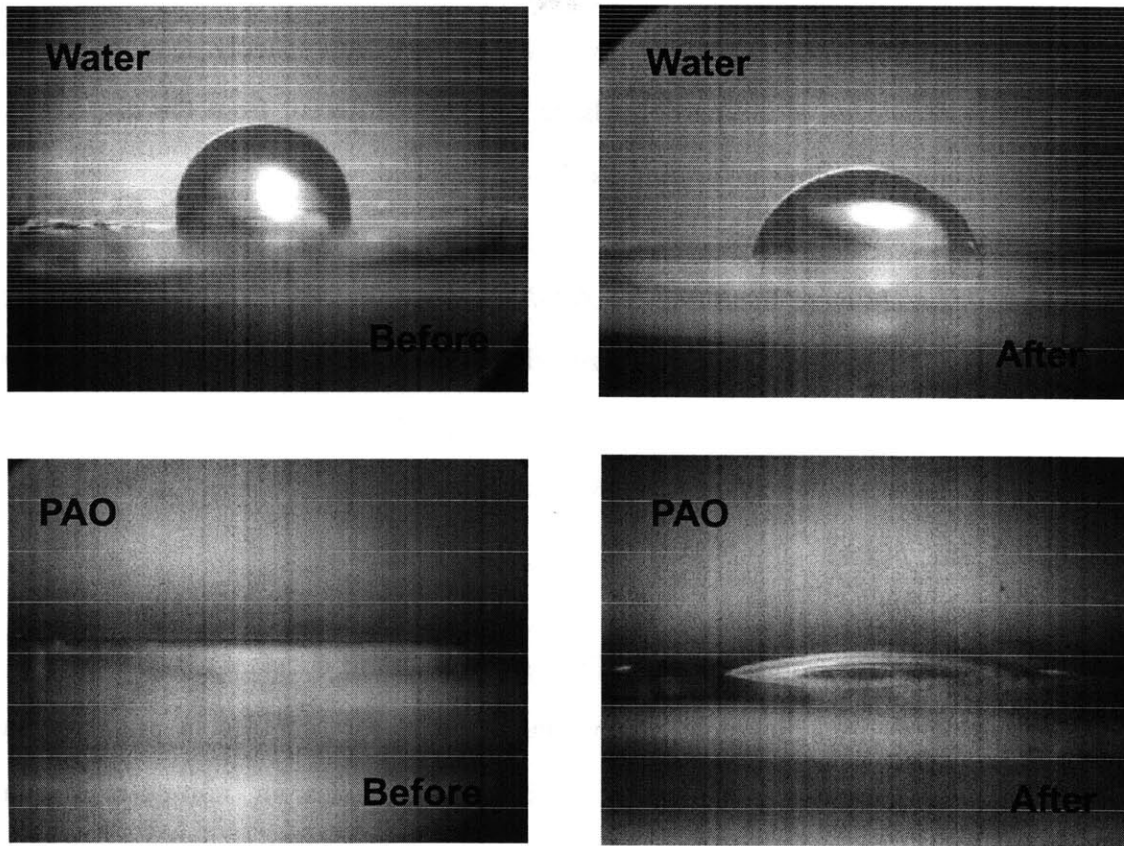


Figure 2-3: The original graphite flakes without any treatment are hydrophobic to water but hydrophilic to oil. After microwave expansion, they become much less hydrophobic to water and less hydrophilic to oil. This behavior is because the microwave expansion treatment brings new functional groups to the surfaces of graphite flakes.

Figure 2-2 shows the graphite flake's hydrophilicity/hydrophobicity to water and PAO before and after microwave expansion. We can see that the treatment has the potential to increase the stability of water based graphite suspensions since it decreases the hydrophobicity to water. To more accurately determine the best microwave time for the graphite particles, we choose different microwave times (5 sec, 30 sec, 60 sec, 120 sec, and 180 sec) to measure the zeta potential of graphite particles in different base fluids. Zeta potential is a very important parameter to determine the stability of colloidal suspensions. The dividing line between stable and unstable suspensions [56] is generally taken at either +30mV or -30mV. Particles with zeta potentials more

positive than +30mV or more negative than -30mV can usually lead to stable suspensions. However, if the particles have a density different from the dispersant, they will eventually sediment forming a close packed bed.

The zeta potentials were measured by *ZetaPALS* (Zeta Potential Analyzer Utilizing Phase Analysis Light Scattering). It utilizes Phase Analysis Light Scattering (PALS) to determine the electrophoretic mobility of charged particles [57]. Meanwhile the zeta potential can be calculated using the Henry equation [58]:

$$U_E = \frac{2\varepsilon\zeta f(\kappa a)}{3\eta} \quad (2.1)$$

where U_E is the electrophoretic mobility, ε is dielectric constant, η is viscosity, and $f(\kappa a)$ is Henry's function which equals to 1.0 for particles in polar media (Hückel approximation) and equals to 1.5 for particles in non-polar media (Smoluchowski approximation).

Figure 2-3, 2-4, and 2-5 show the measurement results of graphite particles zeta potential in different base fluids. From these results we can see that as the microwave time increases, the absolute values of zeta potential will decrease. Because too long microwave time will cause annealing of defects on the graphite flakes. These results indicate that the suspension stability will decrease as the microwave time increases. Although it is better to choose 5 seconds microwave time for larger zeta potential, we choose 7 seconds microwave time in the experiments because we observed that 5 seconds is too short so that many graphite particles do not have enough time to expand.

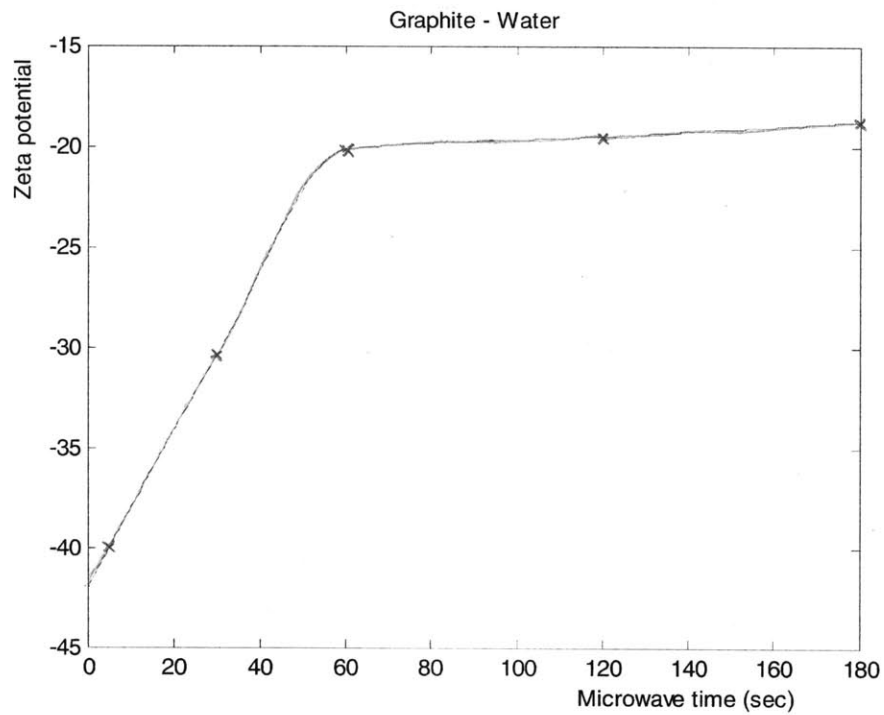


Figure 2-3: Graphite particles zeta potential in DI water as a function of microwave time. The longer microwave time is, the smaller the absolute value of zeta potential is.

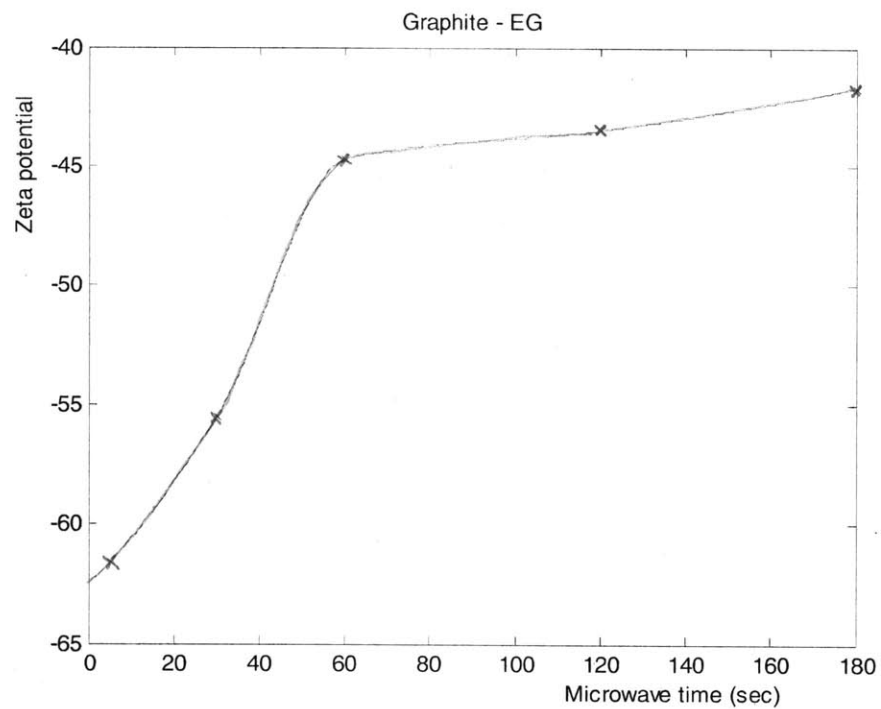


Figure 2-4: Graphite particles zeta potential in ethylene glycol as a function of microwave time. The longer microwave time is, the smaller the absolute value of zeta potential is.

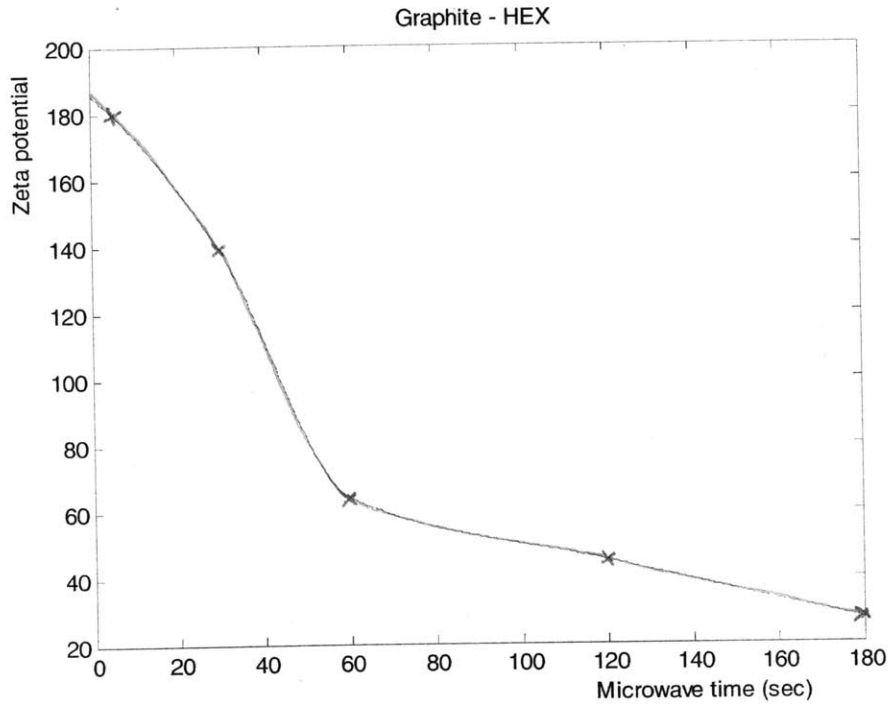


Figure 2-5: Graphite particles zeta potential in hexadecane as a function of microwave time. The longer microwave time is, the smaller the absolute value of zeta potential is.

2.2 Graphite Suspensions Preparation

Expanded graphite flakes were then dispersed into ethylene glycol and other liquids to create graphite suspensions with different volume fractions. To make the expanded graphite disperse uniformly in the base fluids, we must use ultrasonic probe to sonicate the mixture. The probe (SONICS Vibra-Cell VCX 750) was immersed into the suspensions and close to the wall of the container (50ml plastic beaker). And the “Amplitude” parameter keeps at 80% regardless of the varying loading conditions. During the sonication, we also place a stirrer in the sample to make the dispersion process more rapid. The ultrasonic time varies as the graphite volume fraction increases. At low volume fraction, i.e. 0.03%~0.1%, 2 min~4 min ultrasonic time is

enough. However, at high volume fraction, i.e. 0.4%~1%, 12 min~15 min ultrasonic time is chosen in our experiment. Figure 2-6 shows our ultrasonic probe experiment setup.

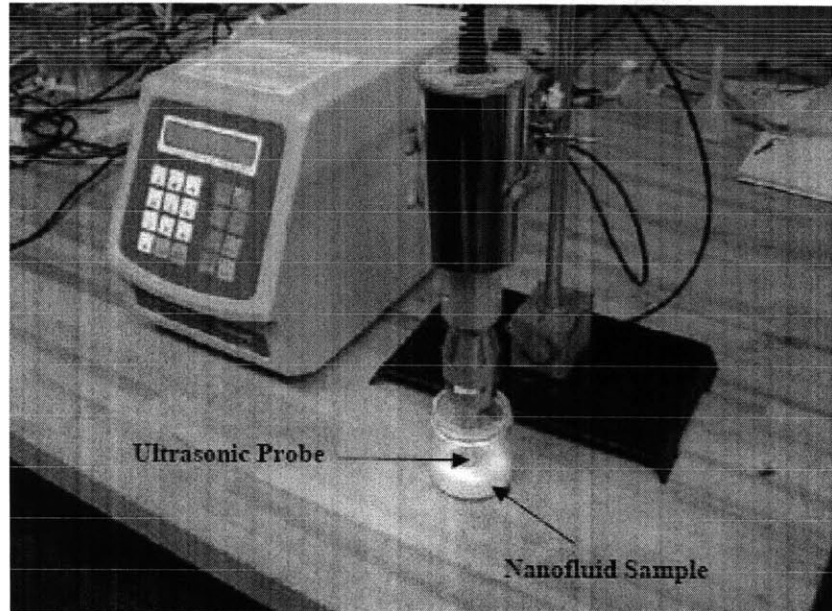


Figure 2-6: Ultrasonic setup. Sometimes when long ultrasonic time is needed, it is better to put the small suspension sample container into a big container which contains cooling water so that the ultrasonic probe and the suspension sample will not be overheated.

As we will see in the next chapter, the thermal conductivity of suspensions will decrease as the ultrasonic time increases. However, too short ultrasonic time will make the samples too viscous, especially at high volume fractions. So there is a tradeoff between high thermal conductivity and low viscosity. Figures 2-7 and 2-8 show the SEM and TEM images of graphite flakes after ultrasonic. The graphite flakes have an average diameter of several microns and thickness from several to several tens nanometers. This is the reason why our samples are called graphite suspensions, not graphite nanofluids.

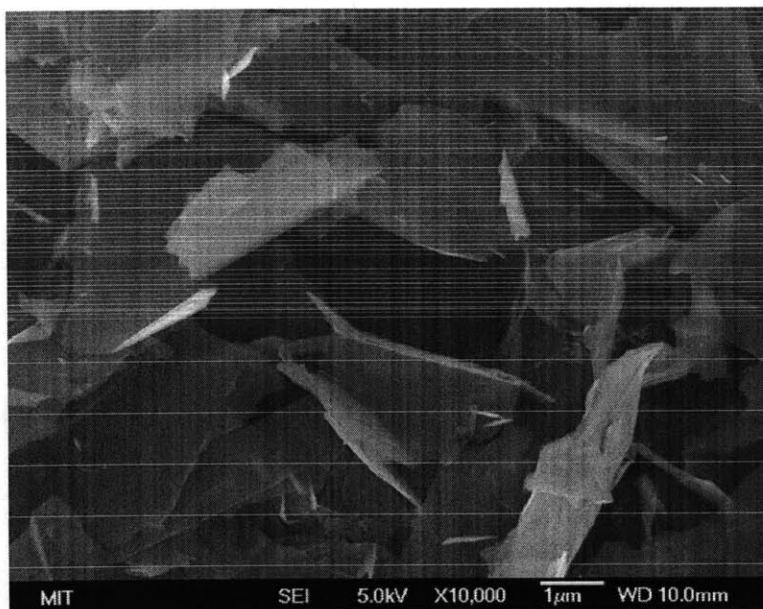


Figure 2-7: SEM image of graphite flakes after ultrasonic preparation.

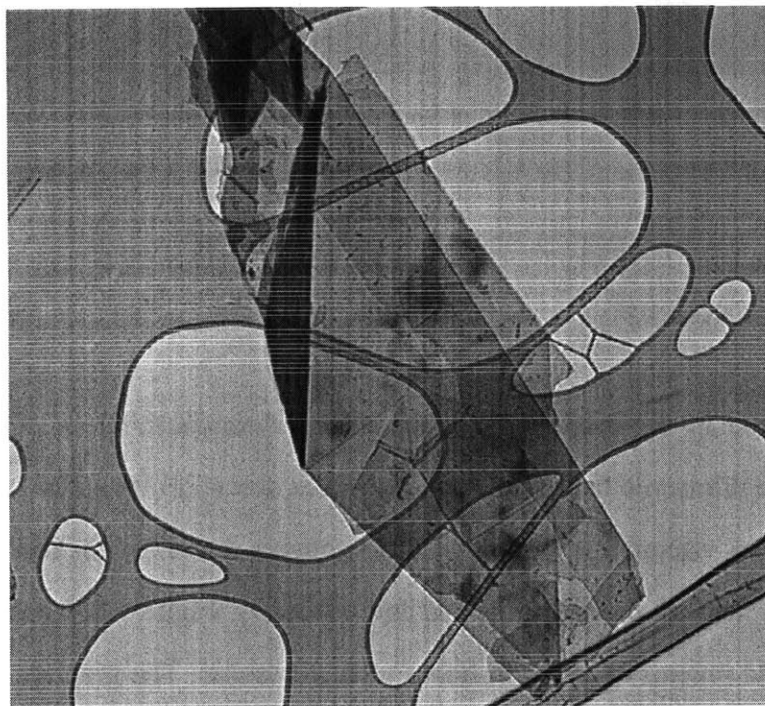


Figure 2-8: TEM image of graphite flakes after ultrasonic preparation.

Using the microwave expansion method and choosing appropriate ultrasonic time, we could obtain very stable graphite suspensions with different base fluids. Figure 2-9 shows that the graphite suspensions do not sediment even after keeping static status for three months.

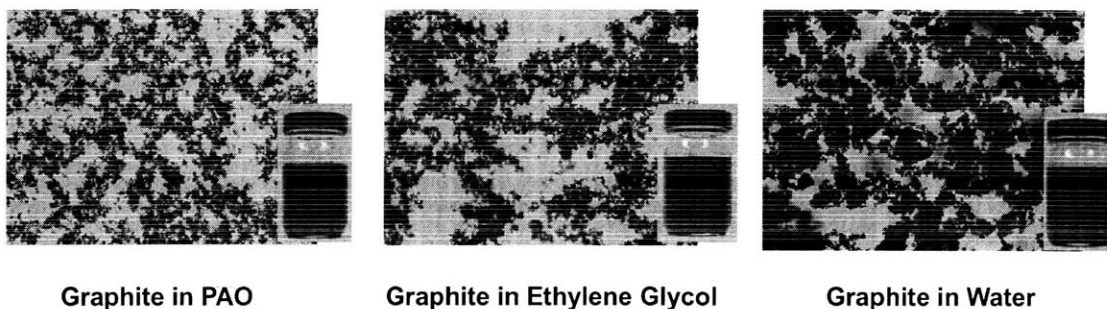


Figure 2-9: Optical images of graphite suspensions with different base fluids: PAO, Ethylene Glycol, and DI water. The small insets are pictures of graphite suspensions samples which were taken three months after the preparation.

2.3 Summary

In this chapter, we overviewed the traditional nanofluids preparation methods and discussed the challenge of nanofluids preparation. To avoid the quick sediment of graphite particles in water, we used microwave expansion method to bring new functional groups to the surface of graphite particles. After this treatment, the graphite flakes become less hydrophobic to water. Based on this method, we could prepare quite stable graphite suspensions.

Chapter 3

The Thermal Conductivity of Graphite

Suspensions

There exist many thermal conductivity measurement methods, including steady-state parallel-plate method [59], transient hotwire method [60-61], 3ω method [62-63], optical thermal lensing method [64], transient optical grating method [65], commercial hot disk and KD2 method [66-68]. Our thermal conductivity measurements are based on the transient hotwire method, which is also the most commonly used method for the liquid thermal conductivity measurement so far. In a recent round-robin study of several different nanofluids with 33 groups participated, the thermal conductivity measurement results of our group are consistent with the results of other groups. In this chapter we will introduce the principle of transient hotwire method, discuss the thermal conductivity measurement results of graphite suspensions, and investigate several factors that might affect the thermal conductivity enhancement of our suspensions.

3.1 Transient Hotwire Method

3.1.1 Measurement Principle

In the transient hotwire measurement, a very thin wire is suspended in an infinite medium (usually it is liquid) whose thermal conductivity is to be measured. During

the measurement, an electric current is passed through the wire, which generates Joule heating and thus a temperature rise in the wire. When the wire is long, the heat flux is along the radial direction of the wire. Obviously, the higher thermal conductivity of the medium, the quicker of the heat dissipates from the wire to the medium and therefore lower temperature rise of the wire. The medium temperature is measured by a thermocouple which is embedded in the measurement cell. A single measurement lasts only 2-5 second to avoid nature convection between the wire and the liquid [60].

3.1.2 Mathematical Derivation

The mathematical derivation described below is mostly adopted from the master thesis [69] of Mr. Jack Ma, a former student in our group. There are several assumptions made in the transient hotwire method: 1) the wire is infinitely long, and is surrounded by an infinite medium; 2) the thermal conductivity of the wire is infinite such that the temperature distribution within the wire is uniform; 3) the wire loses heat radially through conduction alone (no convection) to the medium.

In order to avoid the electrical leakage, the wire is coated with a very thin electrical insulating layer. Then the heat conduction from the wire to the medium is divided into three regions: bare metallic wire, electrical insulating layer, and surrounding medium (see Fig. 3-1).

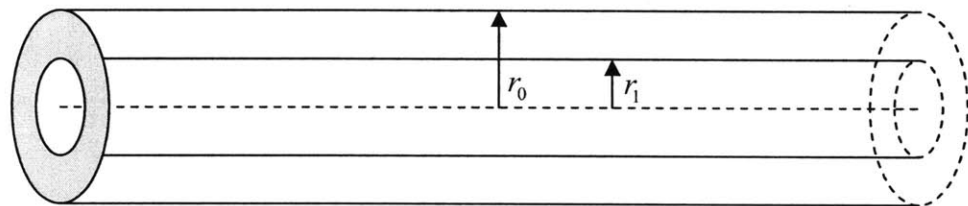


Figure 3-1: Three heat conduction regions: bare metallic wire, electrical insulating layer, and surrounding medium.

The governing heat conduction equations in the cylindrical coordinates in each of the three regions are:

$$\frac{\partial^2 \Delta T_1}{\partial r^2} + \frac{1}{r} \frac{\partial \Delta T_1}{\partial r} - \frac{1}{\kappa_1} \frac{\partial \Delta T_1}{\partial t} = -\frac{q}{\pi r_1^2 k_1} \quad 0 \leq r \leq r_1 \quad (3.1)$$

$$\frac{\partial^2 \Delta T_2}{\partial r^2} + \frac{1}{r} \frac{\partial \Delta T_2}{\partial r} - \frac{1}{\kappa_2} \frac{\partial \Delta T_2}{\partial t} = 0 \quad r_1 \leq r \leq r_0 \quad (3.2)$$

$$\frac{\partial^2 \Delta T_3}{\partial r^2} + \frac{1}{r} \frac{\partial \Delta T_3}{\partial r} - \frac{1}{\kappa_3} \frac{\partial \Delta T_3}{\partial t} = 0 \quad r_0 \leq r \quad (3.3)$$

where r_1 is the radius of metallic wire, r_0 is the radius of coated wire, $\kappa_1, \kappa_2, \kappa_3$ are the thermal diffusivities of the three regions, k_1, k_2, k_3 are the thermal conductivities of the three regions, q is the heat generation per unit length of the wire, and $\Delta T_1, \Delta T_2, \Delta T_3$ are the temperature rises in the three regions.

Since the current only exist in the metallic wire region, there is no heat generation in the other two regions. The initial and boundary conditions for the above heat conduction equations are:

$$\begin{aligned} \Delta T_1 = \Delta T_2 = \Delta T_3 = 0, & \quad t \leq 0 \\ k_1 \frac{\partial \Delta T_1}{\partial r} = k_2 \frac{\partial \Delta T_2}{\partial r}, & \quad r = r_1 \\ k_2 \frac{\partial \Delta T_2}{\partial r} = k_3 \frac{\partial \Delta T_3}{\partial r}, & \quad r = r_0 \\ \frac{\partial \Delta T_1}{\partial r} = 0, & \quad r \rightarrow 0 \\ \Delta T_1 = \Delta T_2, & \quad r = r_1 \\ \Delta T_2 = \Delta T_3, & \quad r = r_0 \\ \Delta T_3 = 0, & \quad r \rightarrow \infty \end{aligned} \quad (3.4)$$

Nagasaka et al. [60] derived an analytical expression for the solution of $\Delta T_1(r, t)$

using the above initial and boundary conditions. Since it has been assumed that the wire has uniform temperature, a spatial average along the radial direction is applied to the solution of $\Delta T_1(r, t)$. Then the average temperature rise in the metallic wire is given by [60]:

$$\overline{\Delta T_1}(t) = \int_0^{r_1} \Delta T_1(r, t) \frac{2\pi r dr}{\pi r_1^2} = \frac{q}{4\pi k_3} \left[\ln t + A + \frac{1}{t} (B \ln t + C) \right] \quad (3.5)$$

where A, B, and C are constants determined by the geometry of the wire, the thermal diffusivity of the three regions, and the thermal conductivity of electrical insulating layer and the medium.

When the diameter of the wire is usually very small, on the order of microns, the term $\frac{1}{t} (B \ln t + C)$ will be much smaller than the constant A. Thus there exists a linear relation between $\overline{\Delta T_1}$ and $\ln t$:

$$\overline{\Delta T_1} = \frac{q}{4\pi k_3} [\ln t + A] \quad (3.6)$$

The slope of the line $\frac{d\overline{\Delta T_1}}{d \ln t}$ is $\frac{q}{4\pi k_3}$, therefore the thermal conductivity of the medium is given by

$$k_3 = \frac{q}{4\pi} \frac{1}{\frac{d\overline{\Delta T_1}}{d \ln t}} \quad (3.7)$$

3.1.3 Experiment Setup

Figure 3-2 shows the thermal conductivity measurement cell. An isonel-coated (acting as an insulating layer) platinum wire is suspended horizontally in the fluid. The reason

why we choose platinum is because it has very accurate temperature coefficient. In our experiments, the diameter of platinum wire is about $25 \mu\text{m}$, and the thickness of Isonel coating is about $1.5 \mu\text{m}$. Since we have assumed that the wire is infinite long, this assumption can be considered valid when the ratio of the wire length to the diameter is above 1500 [70]. In our case, the length of the wire is around 10cm, and then the ratio is about $\frac{10\text{cm}}{25 \times 10^{-6}\text{m}} = 4000 > 1500$. Therefore the wire can be thought infinite long and ending effect can be ignored. Under this conduction, the one-dimensional heat conduction model holds true. As shown in Fig. 3-2, the resistance of the wire is measured by four-point method. To eliminate the leakage of the electrical current from the contacting points to the fluid, two layers of electrical insulating epoxy are applied to the surfaces of the contacting points [71].

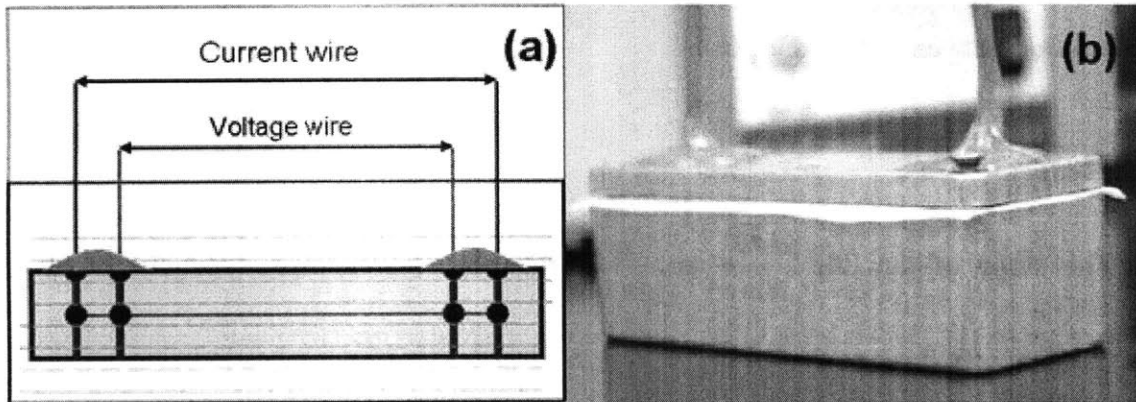


Figure 3-2: Thermal conductivity measurement cell.

The measurement system is shown in Fig. 3-3. A Wheatstone bridge circuit is commonly used for high-accuracy resistance measurement. Two arms of the bridge are consisted of two precision resistors. The other two arms are consisted of the hotwire cell and a potentiometer. In the initial state, the zero output voltage between point A and B is achieved through adjusting the potentiometer. After that, the system starts running and the electrical current is passing through the wire. The experimental duration will last for 2 seconds. When the current passes through the wire, Joule

heating will increase the wire temperature. Thus the resistance of the wire will change consequently, causing a imbalance of the bridge. The data acquisition system will record the voltage variation. Then the wire resistance as a function of time is obtained. Since we already know the temperature coefficient of platinum, the wire temperature as a function of time is also obtained. The fluid thermal conductivity is thus calculated by using Eq. (3.7). The whole transient hotwire measurement setup is shown in Fig. 3-4.

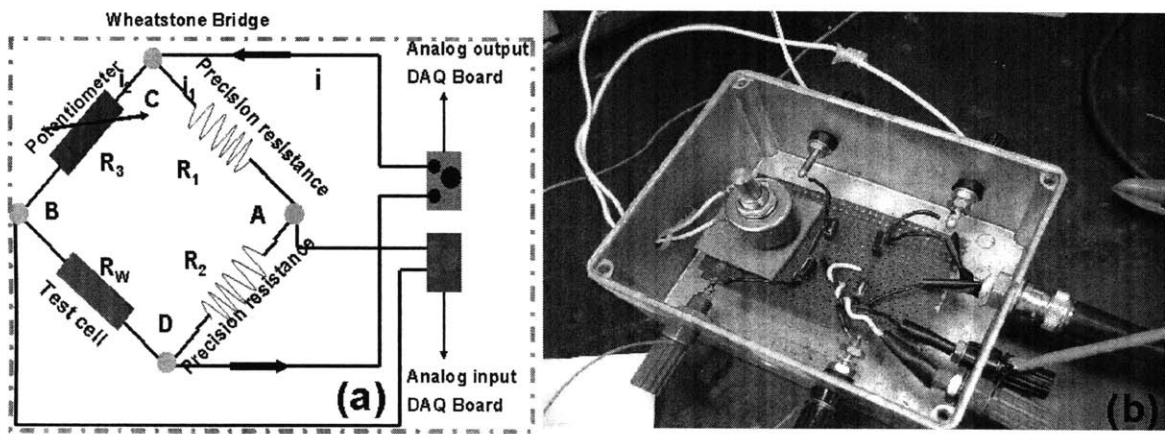


Figure 3-3: Wheatstone bridge circuit for transient hotwire equipment.

The detail calculation of thermal conductivity is described as following:

As shown in Fig. 3-3, the output voltage is the voltage difference between point A and point B.

$$V_{out} = V_A - V_B \quad (3.8)$$

Using the voltage divider relation, V_{out} can be written as

$$V_{out} = V_{in} \left[\frac{R_w + R_p}{R_3 + R_w + R_p} - \frac{R_2}{R_1 + R_2} \right] \quad (3.9)$$

where R_w is the resistance of the hotwire, and R_p is the parasitic resistance associated with the hotwire cell. Let $R_4 = R_w + R_p$ and substitute into Eq. (3.9),

$$V_{out} = V_{in} \left[\frac{R_4}{R_3 + R_4} - \frac{R_2}{R_1 + R_2} \right] = V_{in} \left[\frac{R_4 R_1 - R_2 R_3}{(R_1 + R_2)(R_3 + R_4)} \right] \quad (3.10)$$

Apply Kirchoff's current law at point C,

$$i = i_1 + i_2 = \frac{V_{in}}{R_1 + R_2} + \frac{V_{in}}{R_4 + R_3} = V_{in} \left[\frac{R_1 + R_2 + R_3 + R_4}{(R_1 + R_2)(R_3 + R_4)} \right] \quad (3.11)$$

Eq. (3.11) can also be written as

$$V_{in} = i \left[\frac{(R_1 + R_2)(R_3 + R_4)}{R_1 + R_2 + R_3 + R_4} \right] \quad (3.12)$$

Combine Eq. (3.12) and Eq. (3.10),

$$\begin{aligned} V_{out} &= i \left[\frac{(R_1 + R_2)(R_3 + R_4)}{(R_1 + R_2 + R_3 + R_4)} \right] \left[\frac{R_4 R_1 - R_2 R_3}{(R_1 + R_2)(R_3 + R_4)} \right] \\ &= i \left[\frac{(R_w + R_p) R_1 - R_2 R_3}{(R_1 + R_2 + R_3 + R_w + R_p)} \right] \end{aligned} \quad (3.13)$$

If R_w changes by ΔR_w ,

$$V_{out} + \Delta V_{out} = i \left[\frac{(R_w + \Delta R_w + R_p) R_1 - R_2 R_3}{(R_1 + R_2 + R_3 + R_w + \Delta R_w + R_p)} \right] \quad (3.14)$$

Since Wheatstone bridge is in balance at the initial state, then $V_{out} = 0$, and let

$$R_1 = R_2 = R$$

$$\Delta V_{out} = i \left[\frac{(R_w + R_p - R_3)R + \Delta R_w R}{(2R + R_3 + R_w + \Delta R_w + R_p)} \right] \quad (3.15)$$

ΔR_w can be solved from Eq. (3.15)

$$\Delta R_w = \left[\frac{(R_w + R_p - R_3)R - (2R + R_3 + R_w + R_p) \frac{\Delta V_{out}}{i}}{\frac{\Delta V_{out}}{i} - R} \right] \quad (3.16)$$

Then the temperature rise of the hotwire ΔT_w can be obtained from ΔR_w and the temperature coefficient of resistance of hotwire α ,

$$\Delta T_w = \frac{\Delta R_w}{\alpha} \quad (3.17)$$

The hotwire is made from platinum, which has very accurate temperature coefficient $\alpha = 0.003729 / ^\circ C$. Finally, the thermal conductivity of fluid can be calculated by using Eq. (3.7).

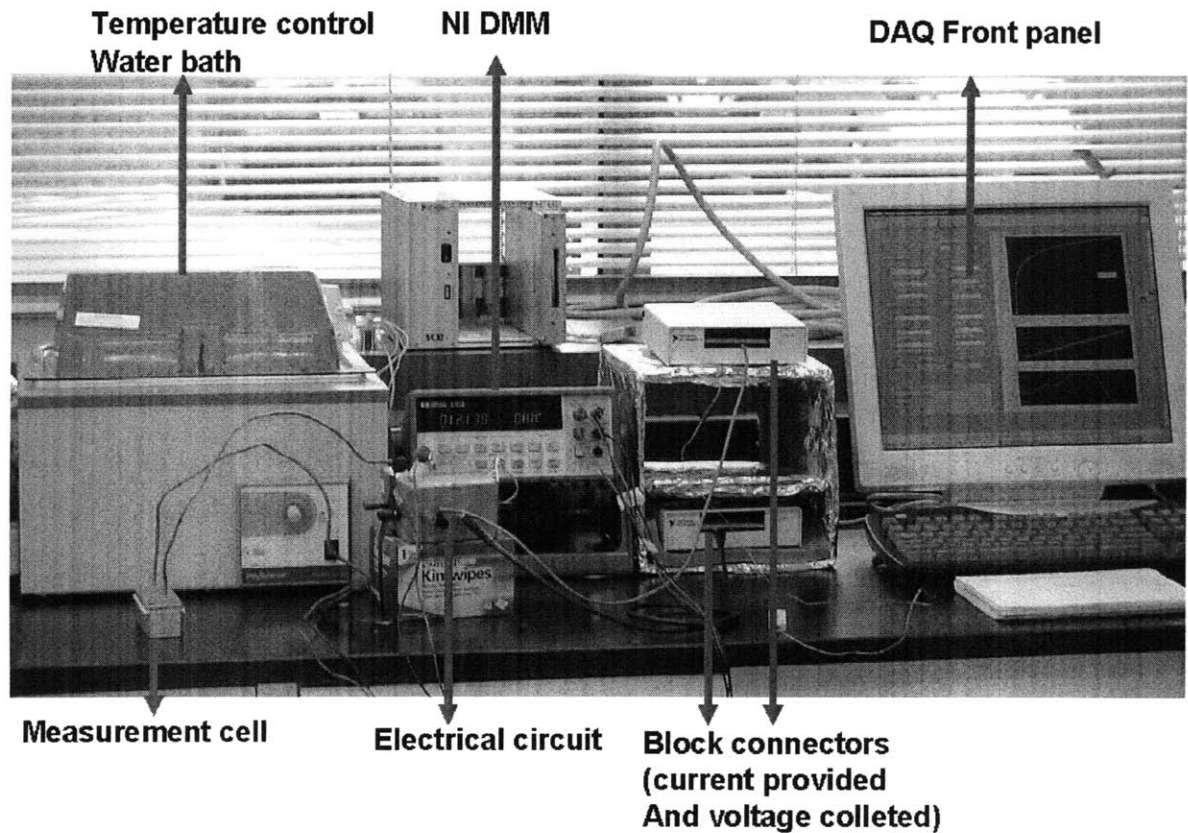


Figure 3-4: Transient hotwire measurement setup.

To make sure the data obtained by our measurement setup is accurate, it is very important to do the system calibration before measuring the thermal conductivity of samples. We calibrate the cell using one standard liquid (pure ethylene glycol) with known thermal conductivity value. A major uncertainty of the length of the hot wire since it is difficult to main a straight line between two supports during wire attachment, and we use calibration to determine its exact length. We initialize the wire length with a suitable value from measurement, and adjust the length till the measured thermal conductivity of this standard liquid equals to the standard value reported in the literature. For the sake of caution, it is better to do a second calibration

test using a different standard liquid (DI water) to see whether the calibrated wire length is the same as or very close to the previous calibrated length. The relative errors between our calibrated thermal conductivity values and the standard values reported in literature are 0.44% for ethylene glycol and 0.57% for DI water. With the proper wire length, we can start to measure the thermal conductivity of our graphite suspensions.

3.2 Thermal Conductivity Enhancement of Graphite Suspensions with Different Base Fluids

The thermal conductivity enhancement of nanofluids (or suspensions) is defined as

$$Enhancement(\%) = \left(\frac{k_{nf}}{k_b} - 1 \right) \times 100 \quad (3.18)$$

where k_{nf} is the thermal conductivity of nanofluids, k_b is the thermal conductivity of base fluid.

We investigated the thermal conductivity enhancement of graphite suspensions with three kinds of base fluids: DI water, ethylene glycol, and PAO. Among the three base fluids, DI water has the highest thermal conductivity, while PAO has the lowest one. Graphite is hydrophilic to oil but hydrophobic to water, in order to get stable water based graphite suspensions, we need do some surface treatment to the graphite particles. This has been introduced in chapter 2.

Figure 3-5 shows the thermal conductivity as a function of graphite volume fraction in three different base fluids. The volume fraction ranges from 0.2% to 1%. Figure 3-6 shows the corresponding thermal conductivity enhancement as a function of graphite volume. Apparently, the addition of graphite particles into the base fluids increases the

fluids thermal conductivity dramatically, and the enhancement increases as the graphite volume fraction increases.

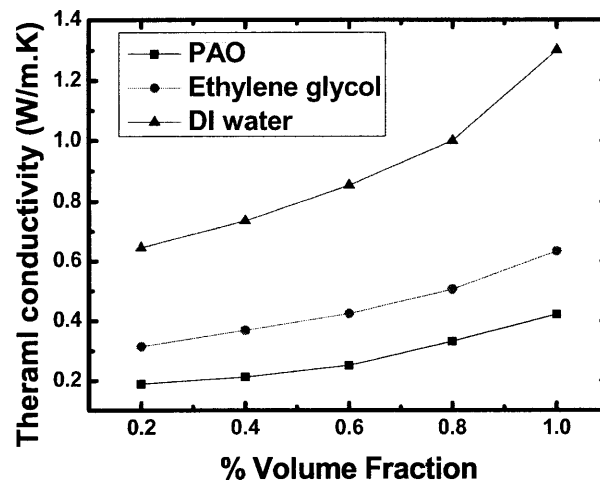


Figure 3-5: The thermal conductivity of graphite suspensions at different volume fraction in three kinds of base fluids.

Shikh et al. [72] reported 160% thermal conductivity enhancement of graphite nanofluids based on PAO at volume fraction of 1%. Choi et al. [10] reported the same thermal conductivity enhancement while using carbon nanotube. For water-base graphite nanofluids, Zhu et al. [73] reported only 12% thermal conductivity enhancement at volume fraction 1%, and Assael et al. [74] reported 38% thermal conductivity enhancement. The thermal conductivity enhancements of our three kinds of graphite suspensions all exceed the maximum values reported in the literatures.

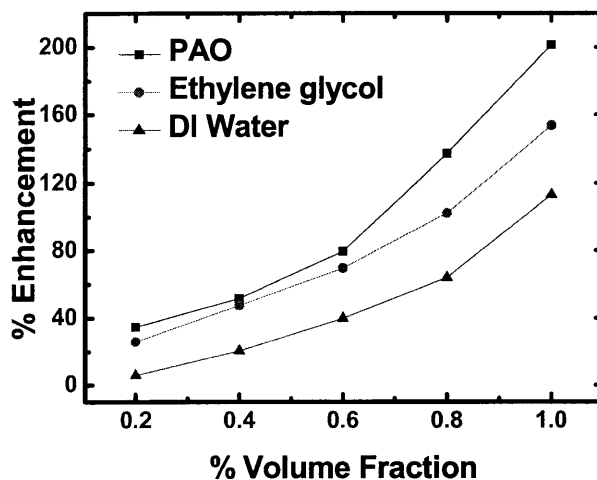


Figure 3-6: The thermal conductivity enhancement of graphite suspensions at different volume fraction in three kinds of base fluids

Graphite suspensions at low volume fraction (lower than 0.2%), especially for the water-base graphite suspensions, are less stable than that at high volume fraction (higher than 0.2%). This is because high volume fraction suspensions contain much more dense graphite clusters, which makes it easier to form a percolation structure within the suspension. As we will discuss more in the next chapter, at low volume fractions, clusters are formed but are separated from each other. At high volume fractions, the clusters become connected to form percolated structures. The percolated structure provides a strong support for the graphite flakes so that they will not settle out for a long time. Figure 3-7 shows the thermal conductivity enhancement of graphite suspensions including data at low volume fraction. It can be seen that the enhancements show different trends at low volume fraction and high volume fraction. The thermal conductivity enhancement increases more quickly at low volume fraction region and slower at high volume fraction region. This might be attributed to the different internal structures of graphite suspensions between low and high volume fraction. Figure 3-7 does not show data for low volume fraction range of the water-based graphite suspensions. Although the surface treatment enables the graphite particles to be a little more hydrophilic to water, this effect is limited. Hence low volume fraction graphite suspensions are still not very stable and data are difficult to

obtain.

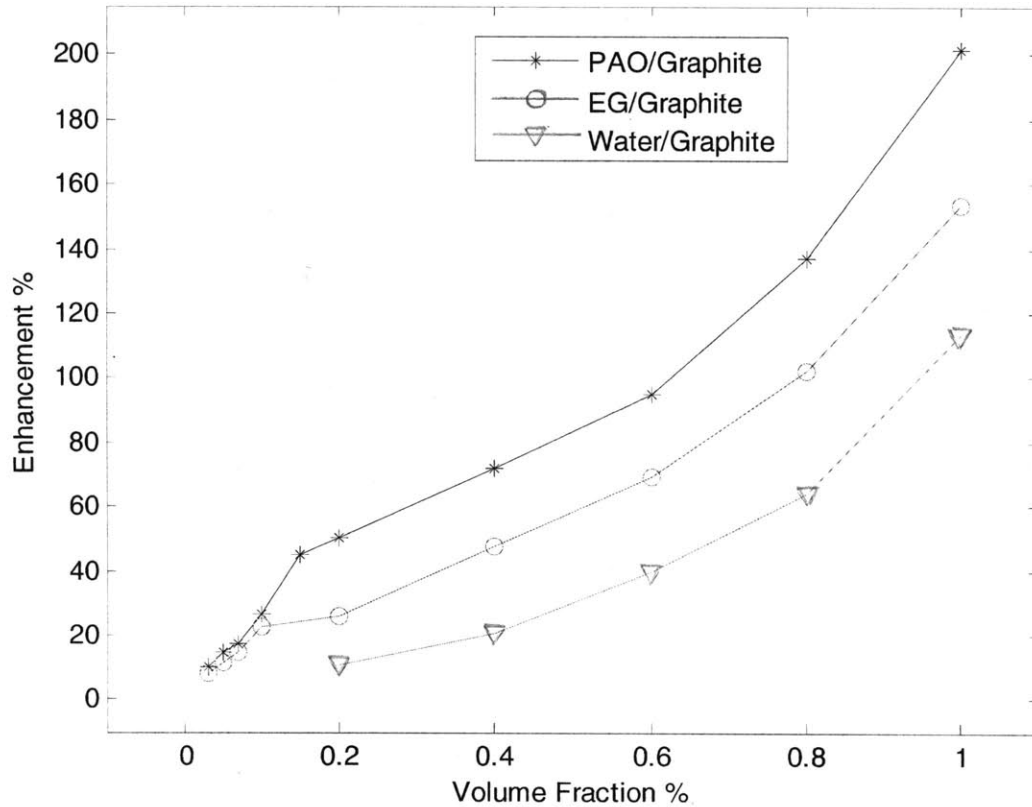


Figure 3-7: The thermal conductivity enhancement of three kinds of graphite suspensions as a function of volume fraction

3.3 The Effect of Microwave Time on the Thermal Conductivity of Graphite Suspensions

In chapter 2, we discussed the microwave-time dependent zeta potential. The zeta potential is a key factor to determine the stability of suspensions, and the stability is a very important factor to decide whether the suspensions can be applied in real world applications.

Different microwave time will cause not only different zeta potential, but also

different thermal conductivity. This is because the microwave process will change the surface structure and charge distribution of graphite flakes. Therefore graphite particles with different microwave time will have different interactions with liquid molecules within the suspensions, leading to a dependence of the thermal conductivity on the microwave time. Figure 3-8 shows the thermal conductivity of PAO-base graphite suspensions (0.2% volume fraction) as a function of microwave time of graphite particles. The inset shows stability of the suspensions at different microwave time. Longer microwave time leads to less stable suspensions, which might due to the annealing of defects on the graphite flakes when the microwave time is too long. The thermal conductivity of graphite suspensions decreases as the microwave time increases.

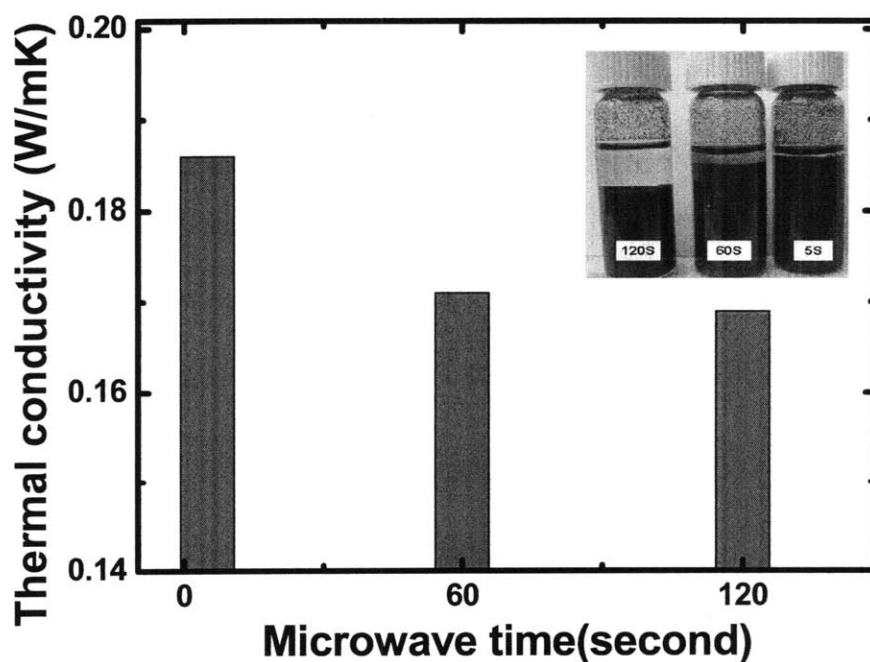


Figure 3-8: Thermal conductivity of PAO/graphite suspensions vs. microwave time.

3.4 The Effect of Ultrasonic Time on the Thermal Conductivity of Graphite Suspensions

Ultrasonication is an important process for graphite suspensions preparation. It makes the graphite particles disperse uniformly in the base fluids. Ultrasonication has two benefits to the suspensions. First, the high power of ultrasonication can break large particles into small pieces, which makes the particles not so easy to settle. Second, the high power of ultrasonication can prevent the agglomeration of particles and thus it is helpful to form stable suspensions. However, too long ultrasonic time will reduce the suspensions thermal conductivity. Take carbon nanotube nanofluids as an example, Xie et al. [75] observed that ultrasonication could reduce the entanglement among those nanotubes, which will increase the thermal conductivity. As the ultrasonic time increases, the sonication power will also break the carbon nanotube into pieces, which will decrease the thermal conductivity. Similar situation occurs for graphite suspensions. The ultrasonication power breaks multilayered graphite flakes into fewer layered or single layered graphite flakes, which increases the aspect ratio of the flakes and reduces the graphite flake size, so it increases the stability of the graphite suspensions. However, like the carbon nanotubes, too long ultrasonic time will break the graphite flakes into small pieces in the lateral dimension, and sometime will also generate some defects on the graphite flakes. All these will decrease the graphite suspension thermal conductivity.

Figure 3-9 shows the thermal conductivity enhancements of three kinds of graphite suspensions as a function of the ultrasonic time. We can see that ultrasonic time has a great influence on thermal conductivity enhancement of suspensions. The thermal conductivity enhancement can decrease significantly as the sonication time is long enough.

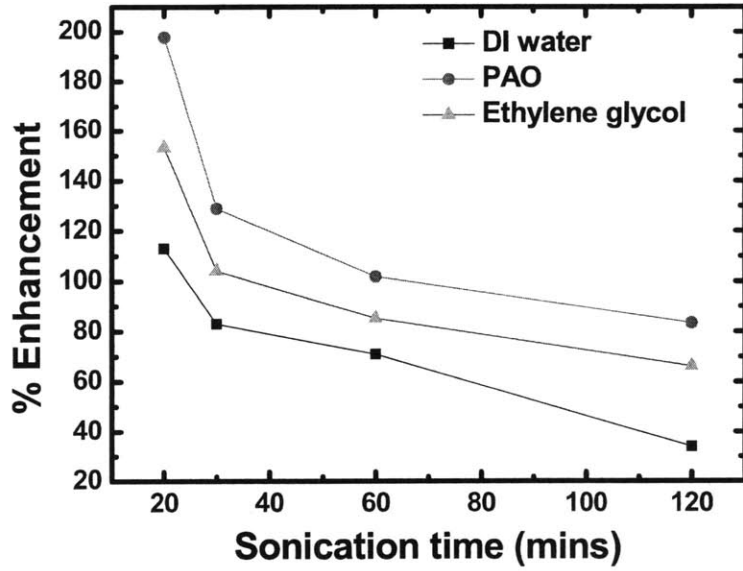


Figure 3-9: Thermal conductivity enhancement as a function of sonication time.

Figures 3-10, 3-11, 3-12 show the SEM images of graphite sample after different ultrasonic times. We may see that the average graphite flake thickness and diameter decreases as the ultrasonic time increases.

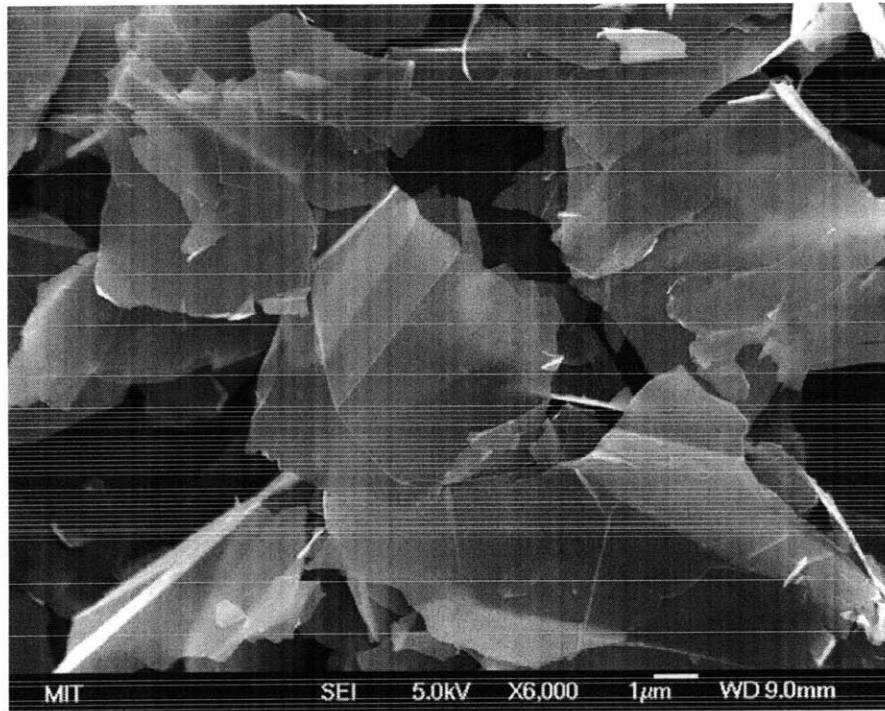


Figure 3-10: SEM image of graphite flakes after sonicating 20 minutes. The average graphite flake diameter is about $7.3 \mu m$ based on the statistics from SEM image.

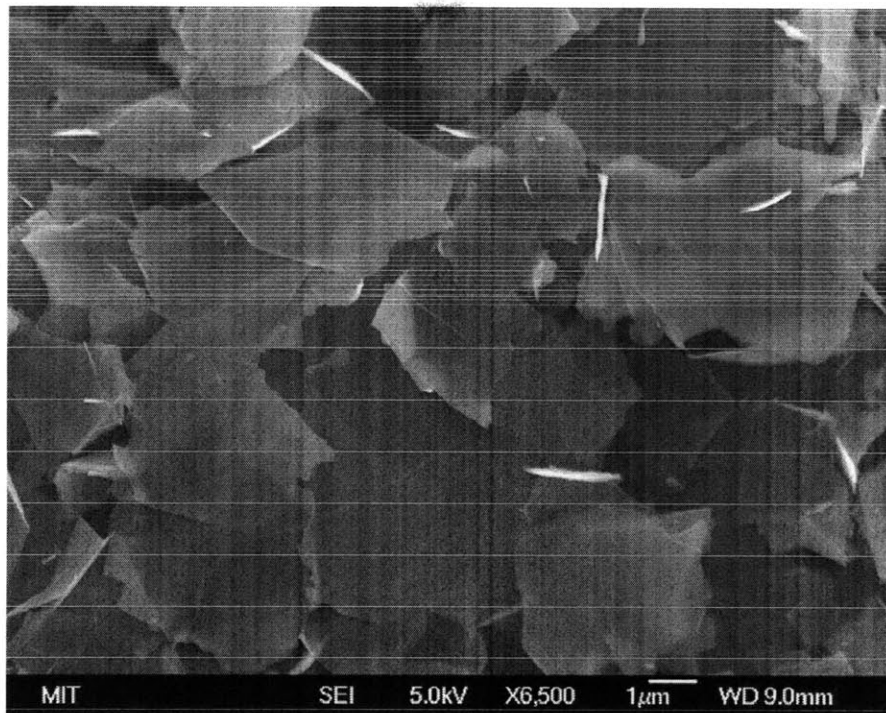


Figure 3-11: SEM image of graphite flakes after sonicating 60 minutes. The average graphite flake diameter is about $4.1 \mu\text{m}$ based on the statistics from SEM image.

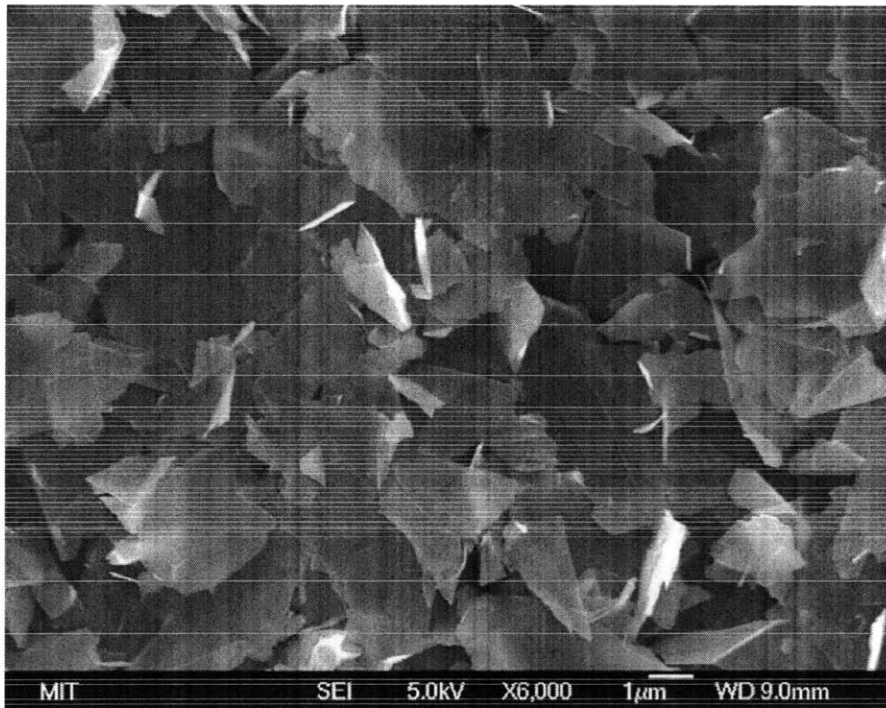


Figure 3-12: SEM image of graphite flakes after sonicating 120 minutes. The average graphite flake diameter is about $1.9 \mu\text{m}$ based on the statistics from SEM image.

From the above discussion, we know that the thermal conductivity of graphite suspensions is influenced by many factors, especially by the preparation processes, such as the microwave time, and the ultrasonic time. It should be mentioned that surfactant weight fraction within the fluid, fluid temperature can also influence the thermal conductivity of the suspensions [15, 76, 77]. The surfactant contained in the suspensions will decrease the thermal conductivity since it introduces new thermal interface resistance between the particles and fluid, and the thermal conductivity of surfactant is also very low. Figure 3-13 is evidence that the suspension thermal conductivity is greatly influenced by the ultrasonic time. Adjusting the ultrasonic time can get higher or lower thermal conductivity. The ultrasonic time varies from 3 minutes to over 35 minutes.

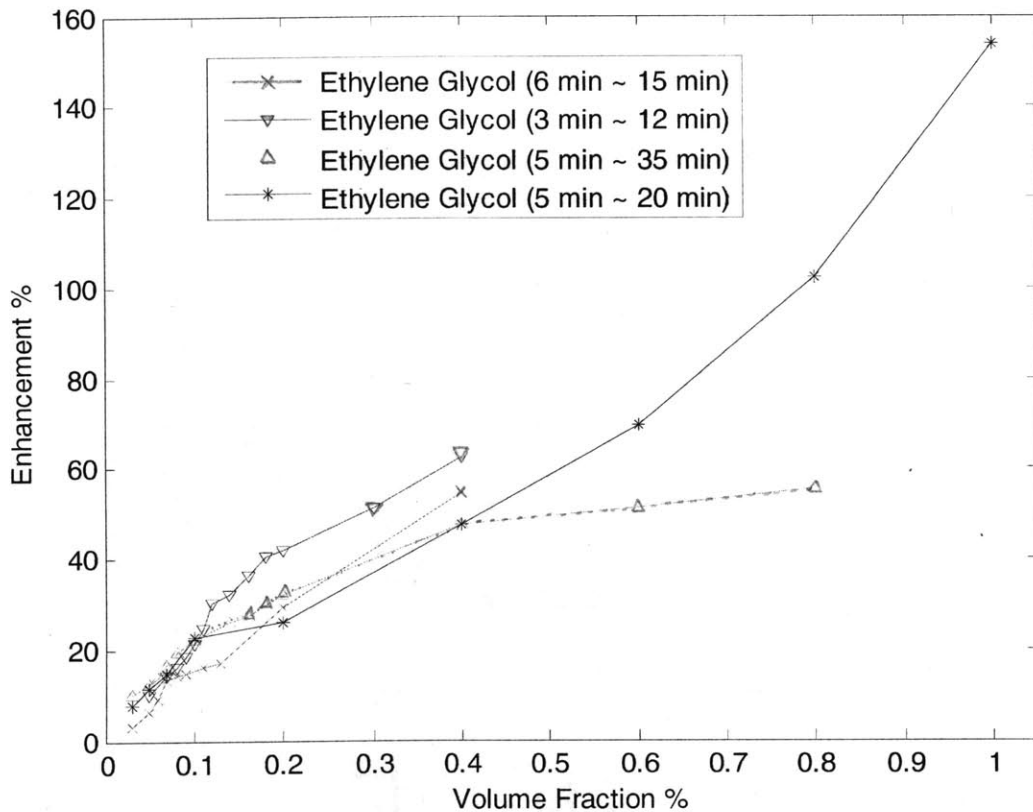


Figure 3-13: Several sets of data on the thermal conductivity enhancement of ethylene glycol based graphite suspensions. These sets of suspension samples were prepared by the same method but using different ultrasonic times. Generally, higher volume fraction samples were prepared

using longer ultrasonic time; lower volume fraction samples were prepared using shorter ultrasonic time. For the same volume fraction samples, we adjusted the ultrasonic time to control the thermal conductivity to be a little higher or lower.

To get comparable data, we should make sure the samples with different volume fraction are prepared by using the same ultrasonic time. Diluting the sample from higher volume fraction to lower volume fraction can satisfy this requirement. Figure 3-14 shows two sets of such data using different ultrasonic time, one set is about 30 minutes, and the other set is about 25 minutes. Both sets of data are compared with one typical curve in Fig. 3-13 in which each volume fraction sample is prepared by using different ultrasonic time.

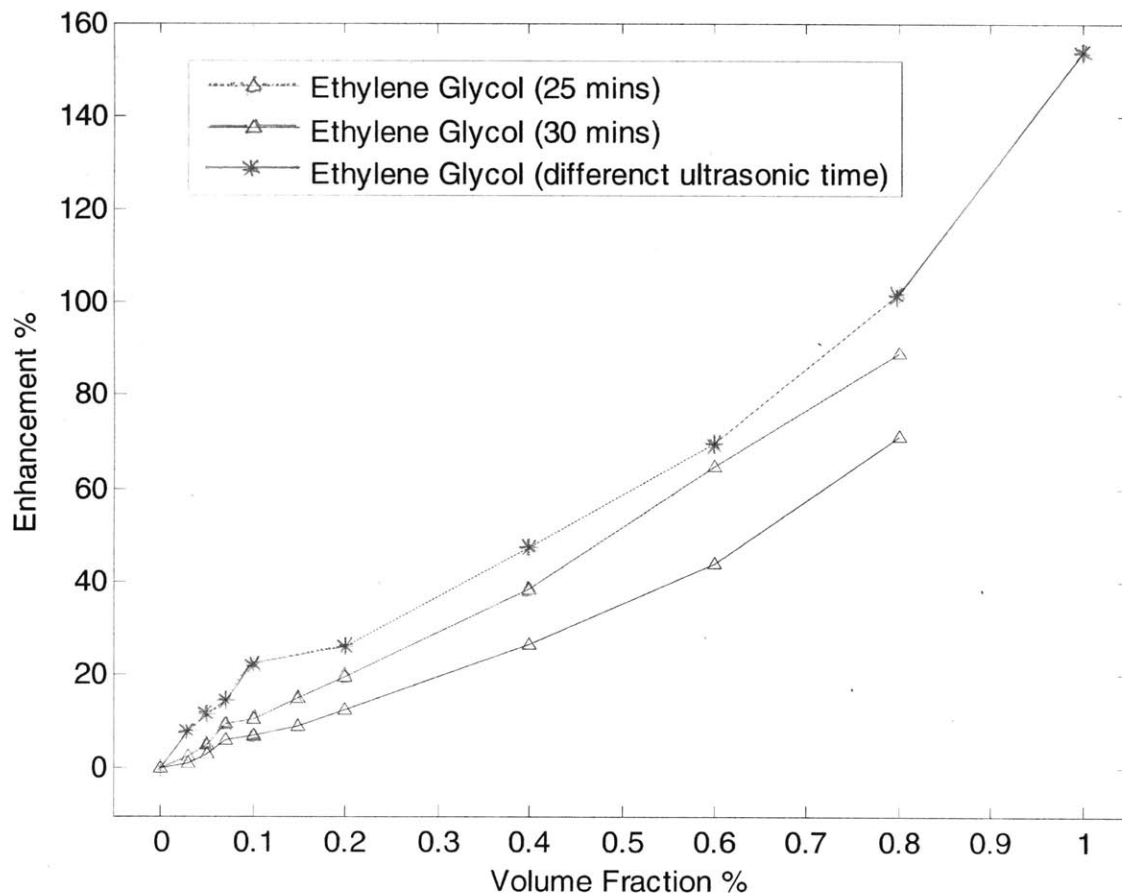


Figure 3-14: Comparison of the thermal conductivity of ethylene glycol based graphite suspensions which are prepared using different ultrasonic time. For the blue curve, the ultrasonic

time of each sample is about 25 minutes. For the black curve, the ultrasonic time of each sample is about 30 minutes. For the red curve, the ultrasonic time of each sample is different. Obviously the ultrasonic time strongly affects the thermal conductivity of graphite suspensions. And the longer ultrasonic time is, the smaller thermal conductivity will be.

3.5 Summary

We introduced the thermal conductivity measurement principle, measured the thermal conductivity enhancements of our graphite suspensions. The results are very exciting since the thermal conductivity enhancements exceed the maximum values reported in the literatures. And we also investigated several factors which might affect the thermal conductivity enhancement of graphite suspensions, including the base fluid materials, the microwave time, and the ultrasonic time, etc. Microwave time mainly changes the surface charge distribution of graphite flakes, and ultrasonic time changes the size of graphite flakes. Therefore the enhancement changes due to microwave time and ultrasonic time can be attributed to the change of internal structures within graphite suspension.

Chapter 4

Study of Graphite Suspensions Using AC

Impedance Spectroscopy

In chapter 3, we investigated the thermal transport properties of graphite suspensions. In this chapter, we will focus on the electrical transport properties of graphite suspensions. The electrical conductivity of graphite is very high, while the electrical conductivity of base fluids (ethylene glycol, PAO, and DI water) are electrically insulating or with low electrical conductivity. When they form suspensions, the internal structures should be very important for the electrical transport properties. Studies of electrical transport properties will help understand the transport mechanisms. One of the most commonly used techniques to investigate the electrical properties of liquid (electrolyte) is AC impedance spectroscopy. Impedance spectroscopy (IS) is a powerful method for the characterization of electrode processes and complex interfaces [78]. It can be used to investigate the dynamics of bound or mobile charge in the bulk or interfacial regions of solid or liquid materials, including ionic, semiconducting, mixed electronic-ionic, and even insulators (dielectrics) [79]. In this chapter, we will apply AC impedance spectroscopy to understand the heat conduction mechanisms of graphite suspensions. For a typical graphite suspension, it contains huge amount of clusters (Fig. 4-3, 4-4, and 4-5 provide clear evidences). The cluster itself can exhibit resistance and capacitance effect, and it can also exhibit resistance and capacitance effect between two clusters. When the volume fraction of the suspension is high, the clusters will connect with each other to form a network percolation structure. Then the suspension might exhibit different resistance and

capacitance effects, as we have observed different increasing slopes of thermal conductivity enhancement curve at different volume fraction ranges. These resistance and capacitance information could be extracted by analyzing the responses of graphite suspensions to a periodic small amplitude AC signal. We are expecting that electrical transport mechanisms investigation could give us some insights on the thermal transport mechanisms.

4.1 AC Impedance Theory

The well known Ohm's law

$$R = \frac{V}{I} \tag{4.1}$$

describes the behavior of an ideal resistor. This relationship tells us the resistance is independent of frequency and the AC voltage and current passing through a resistor are always in phase with each other.

However, real system (e.g. graphite suspensions) exhibits more complex behavior. For instance, graphite clusters can exhibit not only resistance behavior but also capacitance behavior since separated graphite flakes with surface charges on them can be considered as micro-capacitors. For systems with both resistors and capacitors, AC impedance spectroscopy is a very useful tool. Usually the resistance effect within the system can be detected by DC signal or AC signal. However, the capacitance effect can only be detected by AC signal. And these resistance and capacitance effects are determined by the internal structures of the systems. To fully understand the transport mechanisms of graphite suspensions, we must first understand their internal structures. Therefore the AC impedance spectroscopy supplies a useful tool for our purpose.

Usually the electrical behavior of a liquid system is measured by applying the AC

voltage to it and measuring the current through the system. If the applied AC potential is

$$V = V_0 e^{i\omega t} \quad (4.2)$$

and the current response is

$$I = I_0 e^{i(\omega t - \varphi)} \quad (4.3)$$

Then the AC impedance is defined as

$$Z(\omega) = \frac{V}{I} = Z_0 e^{i\varphi} = Z_0 (\cos \varphi + i \sin \varphi) \quad (4.4)$$

where V_0 and I_0 are the amplitudes of the potential and the current, ω is the frequency, and φ is the phase-shift of current response relative to the potential signal. So the expression of AC impedance $Z(\omega)$ is composed of two parts: real part and imaginary part.

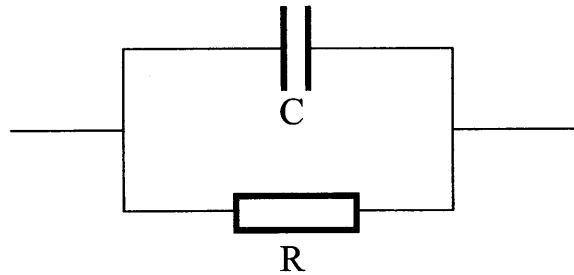


Figure 4-1: A typical electrical circuit – parallel of a resistor R and a capacitor C.

For a typical electrical circuit (see Fig. 4-1, which is also frequently used in the impedance spectroscopy analysis), considered that the impedance of the resistor and a capacitor are R and $1/i\omega C$ respectively, the total impedance of a RC parallel unit is

$$\begin{aligned} Z &= \left(\frac{1}{R} + i\omega C \right)^{-1} = \frac{R}{1 + i\omega RC} \\ &= \frac{R(1 - i\omega RC)}{(1 + i\omega RC)(1 - i\omega RC)} \\ &= \frac{R}{1 + \omega^2 R^2 C^2} - i \frac{\omega R^2 C}{1 + \omega^2 R^2 C^2} \\ &= X + iY \end{aligned} \quad (4.5)$$

If we plot the real part on the X-axis and the imaginary part on the Y-axis, then we get the “Nyquist Plot” (see Fig. 4-2). It should be noticed that Y-axis is negative imaginary part of the impedance in the plot. And the frequency is swept from the highest to the lowest. Each point on the Nyquist plot denotes the impedance at that special frequency. The drawback of Nyquist plot is that when one looks at any point on it, one can not tell the corresponding frequency at that point easily. So there is another popular presentation method called “Bode Plot”. It is plotted with log frequency on the X-axis, and both the log of the absolute value of impedance and the phase-shift on the Y-axis. The Bode plot thus can show clear frequency information [80].

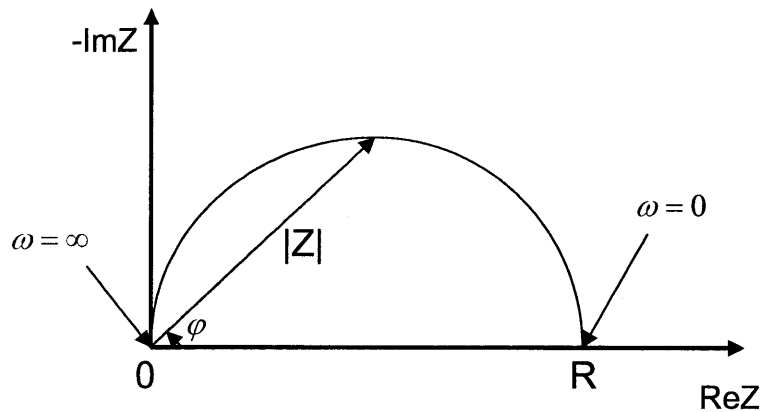


Figure 4-2: The “Nyquist Plot” of the electrical circuit Fig. 4-1.

The Nyquist plot in Fig. 4-2 is a semicircle. This can be demonstrated easily from Eq. (4.5). Since Fig. 4-2 tells us the radius of the semicircle is one half R , therefore we should have

$$\begin{aligned}
\left(X - \frac{R}{2}\right)^2 + Y^2 &= \left(\frac{R}{1 + \omega^2 R^2 C^2} - \frac{R}{2}\right)^2 + \left(-\frac{\omega R^2 C}{1 + \omega^2 R^2 C^2}\right)^2 \\
&= \left[\frac{2R - R(1 + \omega^2 R^2 C^2)}{2(1 + \omega^2 R^2 C^2)}\right]^2 + \left(\frac{\omega R^2 C}{1 + \omega^2 R^2 C^2}\right)^2 \\
&= \frac{R^2(1 - \omega^2 R^2 C^2)^2}{4(1 + \omega^2 R^2 C^2)^2} + \frac{4\omega^2 R^4 C^2}{4(1 + \omega^2 R^2 C^2)^2} \\
&= \frac{R^2(1 - 2\omega^2 R^2 C^2 + \omega^4 R^4 C^4) + 4\omega^2 R^4 C^2}{4(1 + \omega^2 R^2 C^2)^2} \\
&= \frac{R^2(1 + 2\omega^2 R^2 C^2 + \omega^4 R^4 C^4)}{4(1 + \omega^2 R^2 C^2)^2} = \frac{R^2}{4} = \left(\frac{R}{2}\right)^2
\end{aligned} \tag{4.6}$$

The semicircle in a Nyquist plot is characteristic of a single “time constant” ($\tau = RC$). In practical AC impedance measurement, the Nyquist plot usually contains several semicircles, and often only a portion of the semicircle is observable [80].

In most cases, the AC impedance measurement results are much more complex than Fig. 4-2. And a detailed model to describe all the processes which might occur in the system may be too complicated to use. Therefore it is usually analyzed by fitting the figure to an equivalent electrical circuit model. Most of the circuit elements in the model are common electrical elements such as resistors, capacitors and inductors. And usually when constructing the circuit model to approximate the real system, the electrical elements in the model should have physical meanings to stand for certain physical processes or chemical reaction steps. For example, resistance in a circuit represents a conductive path, and a given resistor in the model might represent the solution resistance. And similarly, capacitances and inductances may be associated with space charge polarization regions, adsorption phenomena and electro-crystallization processes at the electrode [79].

Table 4-1 lists the common standard circuit components, the equations for the current versus voltage relationship, and their impedance.

Table 4-1: Standard electrical components

Component	Current v.s. Voltage	Impedance
Resistor	$V = IR$	$Z = R$
Capactor	$I = C(dV/dt)$	$Z = 1/j\omega C$
Inductor	$V = L(dI/dt)$	$Z = j\omega L$

From the above table, it is easy to see that the impedance of a resistor is independent of frequency and has only real part. And the current through a resistor is always in phase with the voltage across the resistor (zero phase-shift). The impedance of a capacitor has only imaginary part and decreases as the frequency increases. And the current through a capacitor has 90 degrees phase-shift with respect to the voltage. The impedance of an inductor also has only imaginary part but increases as the frequency increases. And the current through an inductor has -90 degrees phase-shift with respect to the voltage [80].

The model of a practical electrochemical cell is usually a series and/or parallel combination of circuit elements. The total impedance calculation is the same as series and/or parallel resistance calculation.

For impedance elements in series, the total impedance can be calculated from

$$Z_{series} = Z_1 + Z_2 + Z_3 + \dots \quad (4.7)$$

For impedance elements in parallel, the total impedance can be calculated from

$$\frac{1}{Z_{parallel}} = \frac{1}{Z_1} + \frac{1}{Z_2} + \frac{1}{Z_3} + \dots \quad (4.8)$$

4.2 AC Impedance Measurement and Analysis of Graphite Suspensions

4.2.1 Optical Images of Graphite Particles in Different Base Fluids

Figures 4-4, 4-4, and 4-5 shows the optical images of graphite particles in three different base fluids: PAO, ethylene glycol and DI water, respectively.

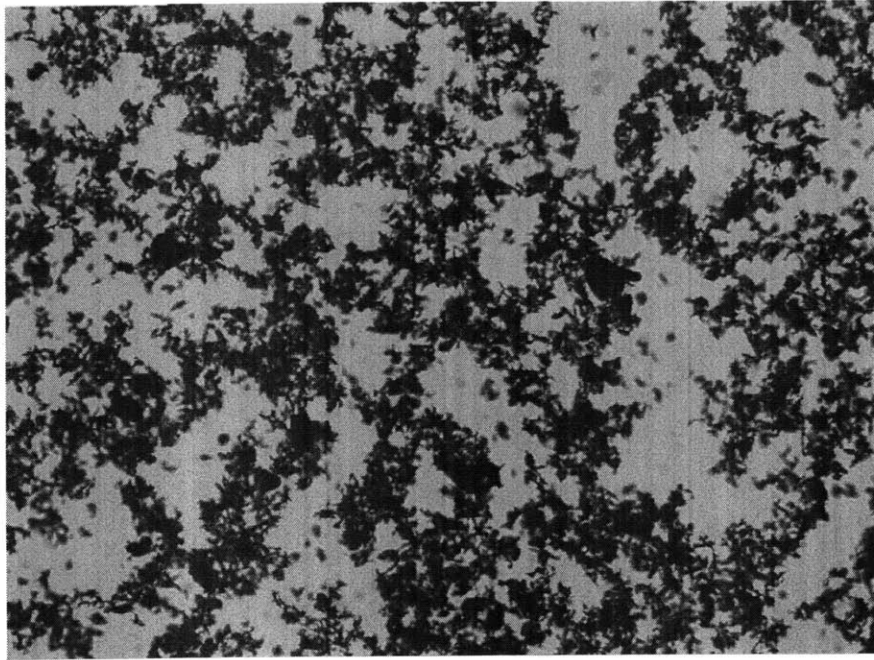


Figure 4-3: Optical image of graphite particles in PAO (vol. fraction: 0.1%)

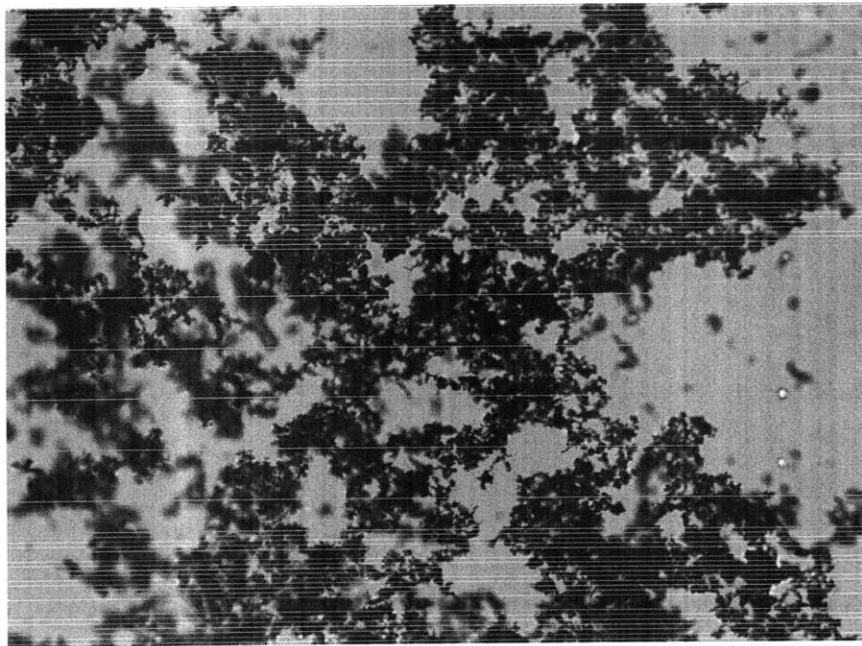


Figure 4-4: Optical image of graphite particles in ethylene glycol (vol. fraction: 0.1%)

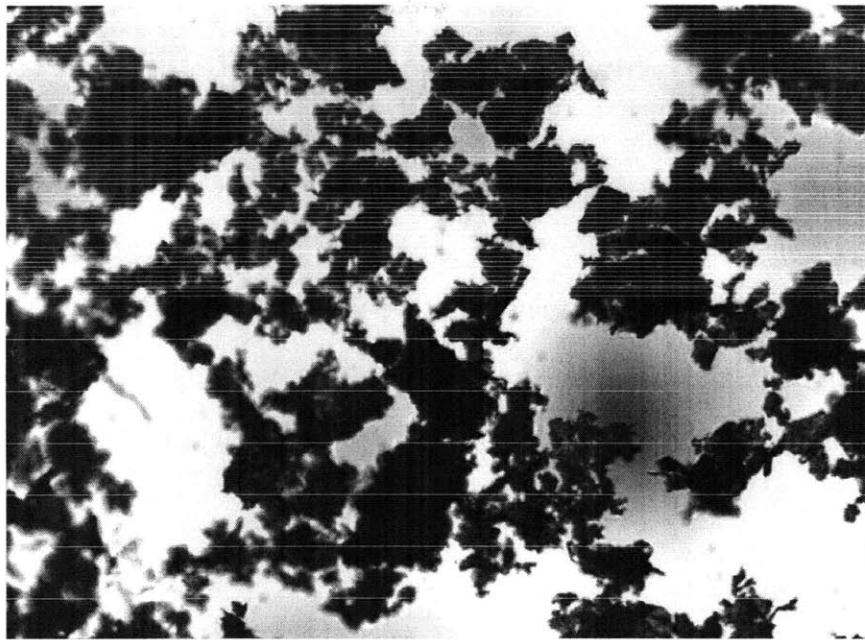
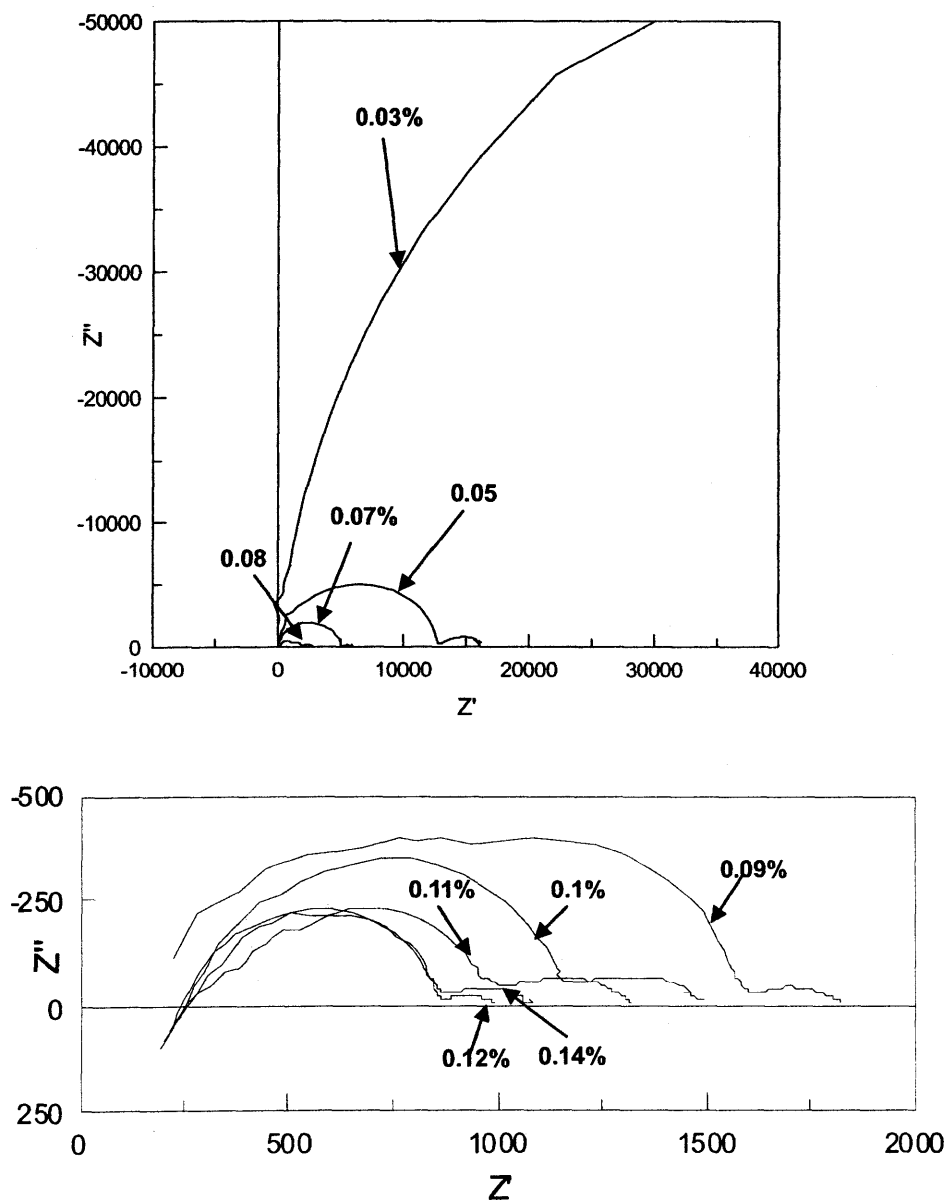


Figure 4-5: Optical image of graphite particles in DI water (vol. fraction: 0.1%)

The optical images show that graphite particles in different base fluids usually form some different structures. This is due to the graphite hydrophobic/hydrophilic properties in different liquids which also determine the stability of graphite suspensions. Nevertheless, there still exist some common characteristics for different graphite suspensions. For example, graphite particles are always likely to form clusters in the fluid. And when the volume fraction increases, the clusters tend to connect to each other to form percolation structures. Because of the graphite hydrophobic/hydrophilic properties vary in different liquids, the percolation structures will start from different volume fractions for different graphite suspensions. Such percolation structures play an important role for enhancing the thermal transport. The difference between electrical transport and thermal transport is that electrical current is more likely passing along the graphite flakes, while heat flux can go through both the graphite flakes and the liquid. However, we believe that the investigation on the electrical transport mechanisms using AC impedance spectroscopy may help us understand the thermal transport mechanisms.

4.2.2 AC Impedance Spectroscopy and Results Analysis

In our experiments, the AC impedances of graphite suspensions were measured by *Model 1260A Impedance / Gain-Phase Analyzer*. It has a wide frequency range from $10 \mu\text{Hz}$ to 32MHz . The frequency range we used is from 10MHz to 0.1Hz . The DC potential is 0, and AC signal amplitude is 10meV . Our experiments are mainly focused on ethylene glycol based graphite suspensions. Figure 4-6 shows a complete set of AC impedance spectroscopy.



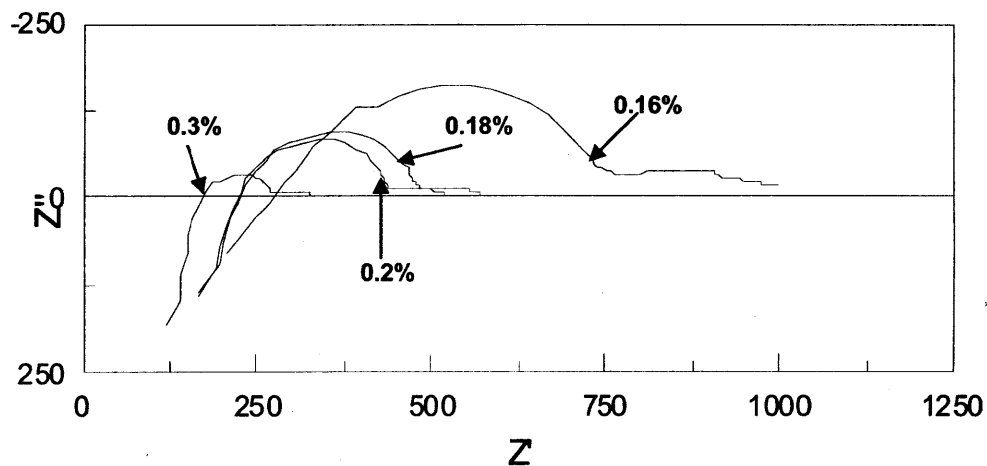


Figure 4-6: Nyquist plots for the AC impedance of ethylene glycol based graphite suspensions with different volume fractions. The X-axis is the real part of the impedance, and the Y-axis is the imaginary part of the impedance. Each curve in this Nyquist plot denotes a specific volume fraction of suspension. These volume fractions are: 0.03%, 0.05%, 0.07%, 0.08%, 0.09%, 0.1%, 0.11%, 0.12%, 0.14%, 0.16%, 0.18%, 0.2%, and 0.3%.

From the above figure we may notice that each curve has sort of semicircle characteristic. It is easy to think of the superposition of several semicircles. Based on this intuitive, we choose a series of three resistor and capacitor parallel units to model the measurement results. Each RC unit has a certain physical meaning. We will specify these meanings in the following example figures.

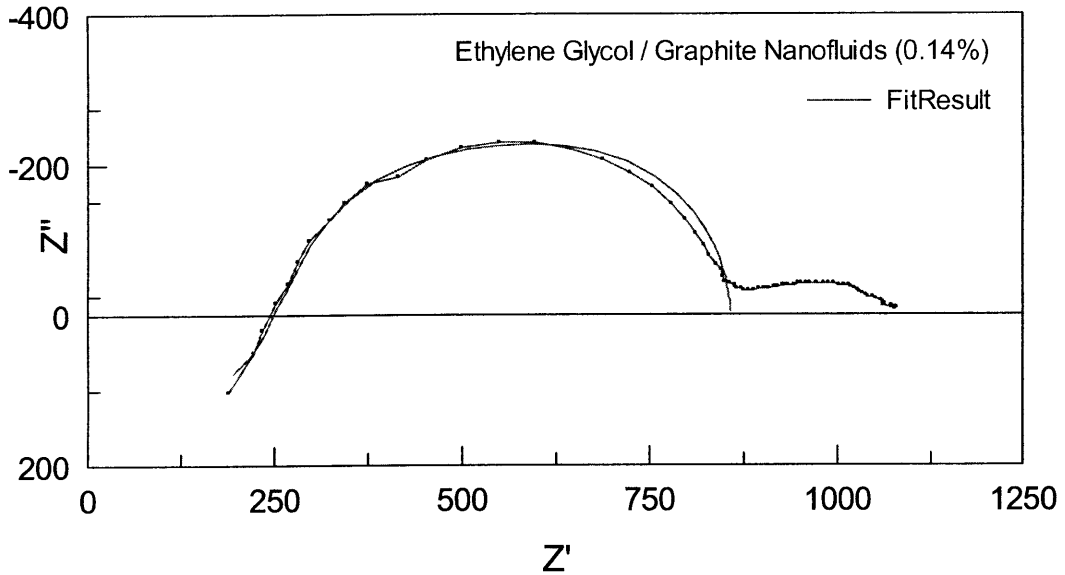


Figure 4-8: An example of AC impedance measurement curve and fitting curve of ethylene glycol based graphite suspension with the volume fraction 0.14%. The fitting curve is based on the model shown in Fig. 4-9.

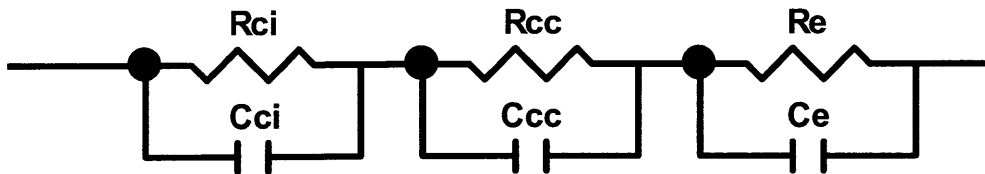


Figure 4-9: The equivalent circuit we used to model the impedance behavior of graphite suspensions. It contains three RC parallel units [51]. The first RC unit denotes for the cluster internal response, where R_{ci} is the cluster internal resistance and C_{ci} is the cluster internal capacitance. The second RC unit denotes for the cluster-cluster response, where R_{cc} is the cluster-cluster resistance and C_{cc} is the cluster-cluster capacitance. The third RC unit denotes for the electrode response, where R_e is the solution resistance and C_e is the double layer capacitance at the electrode.

Using the model we proposed in Fig. 4-9, cluster internal conductance (inverse of

resistance) & capacitance and cluster-cluster conductance & capacitance can be analyzed. We plot them as a function of graphite volume fraction (see Fig. 4-10). The samples used in Fig. 4-10 are corresponding to the magenta curve in Fig. 3-13 which we will redraw in Fig. 4-11.

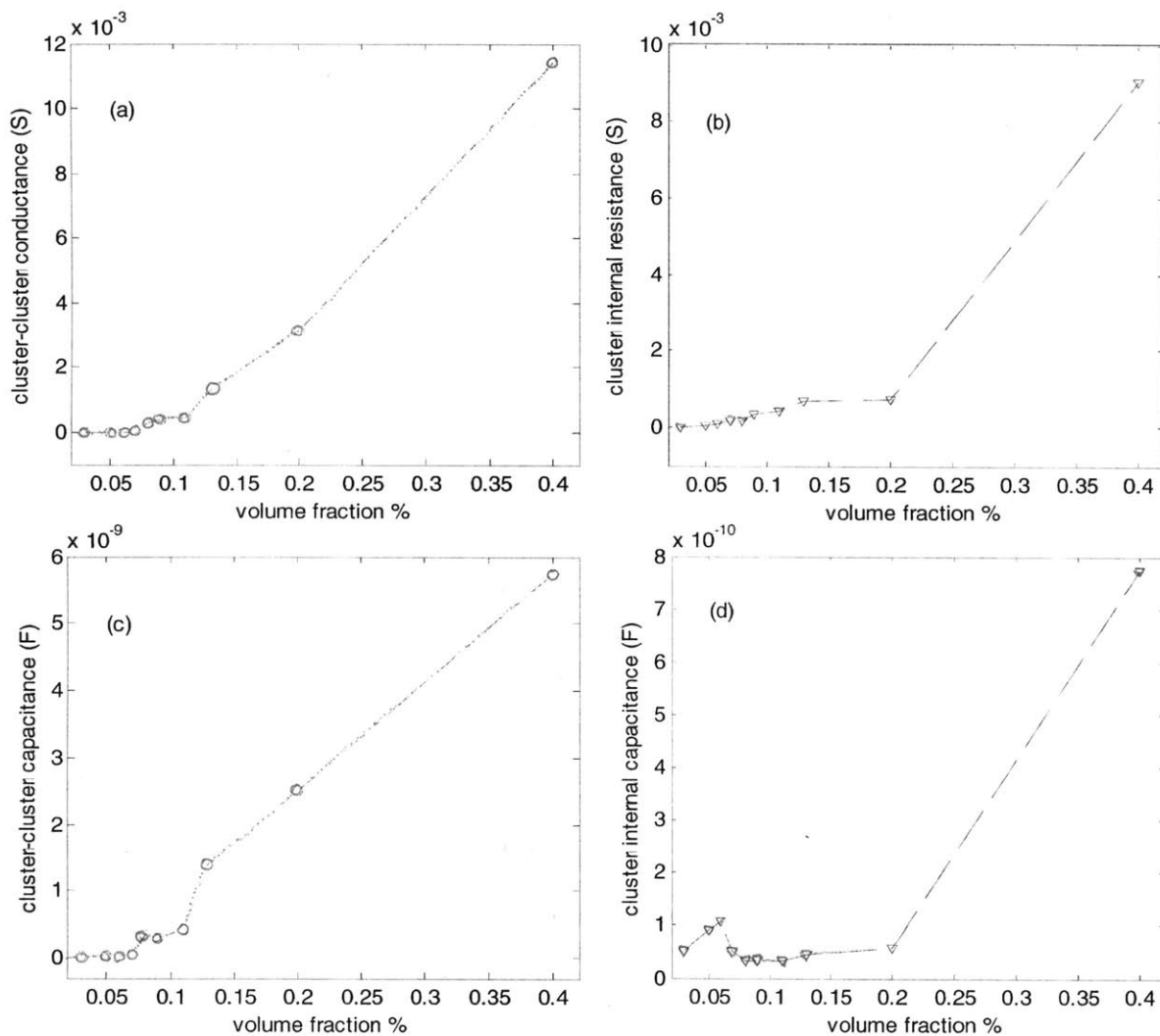


Figure 4-10: Cluster-cluster conductance & capacitance and cluster internal conductance & capacitance as a function of graphite volume fraction in ethylene glycol.

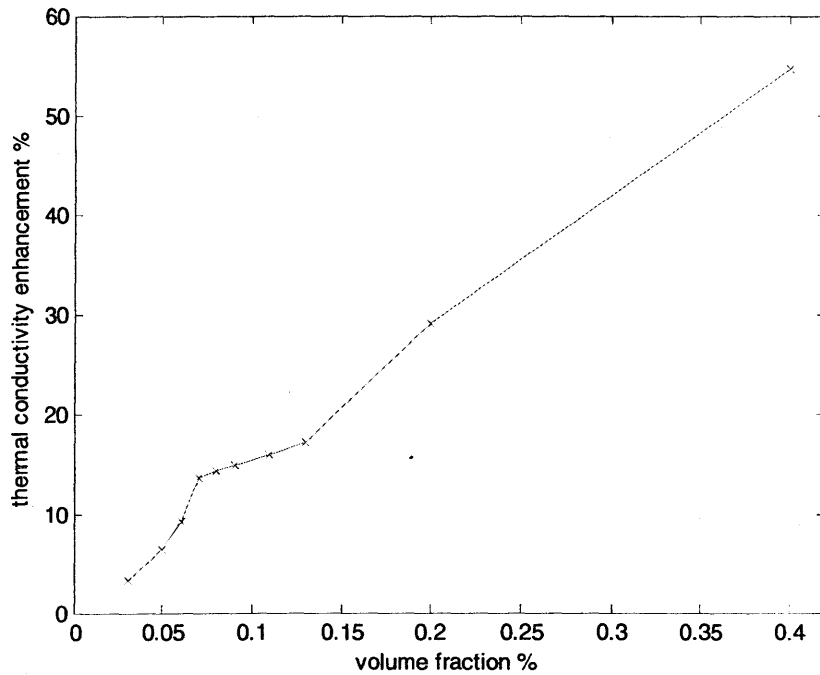


Figure 4-11: Thermal conductivity enhancement of ethylene glycol based graphite suspensions. The samples used in this figure correspond to the samples in Fig. 4-10.

Since the electrical conductivity of graphite is much higher than the base fluid ethylene glycol, both the cluster internal conductance and the cluster-cluster conductance increase as the volume fraction increases (as shown in Fig. 4-10 (a) and (b)). At the same time, when the volume fraction increases, the clusters become closer to each other. Once the clusters are all connected to each other (percolated), the cluster-cluster conductance will increase very quickly, as it is shown in Fig. 4-10 (a).

The drawback of Fig. 4-10 (a) and (b) is that it does not give a clear conductance picture when the volume fraction is low. This drawback can be avoided if plotted in logarithm scale (see Fig. 4-12). In Fig. 4-12 (a), the conductance increases dramatically in the range of 0.07% ~ 0.09%. This range is probably the percolation starting point. In the percolation region, the logarithm of cluster-cluster conductance should be linear with the logarithm of volume fraction $\log K = n \log(\phi - \phi_0) + c$ (or $K = C(\phi - \phi_0)^n$). K is the cluster-cluster conductance, ϕ is the volume fraction and ϕ_0 percolation starting volume fraction. If we choose the percolation starting to

be 0.07%, the percolation relation can be plotted as Fig. 4-13. These points show good linear relation except at only one point. The electrical transport properties do have some connections with thermal transport properties.

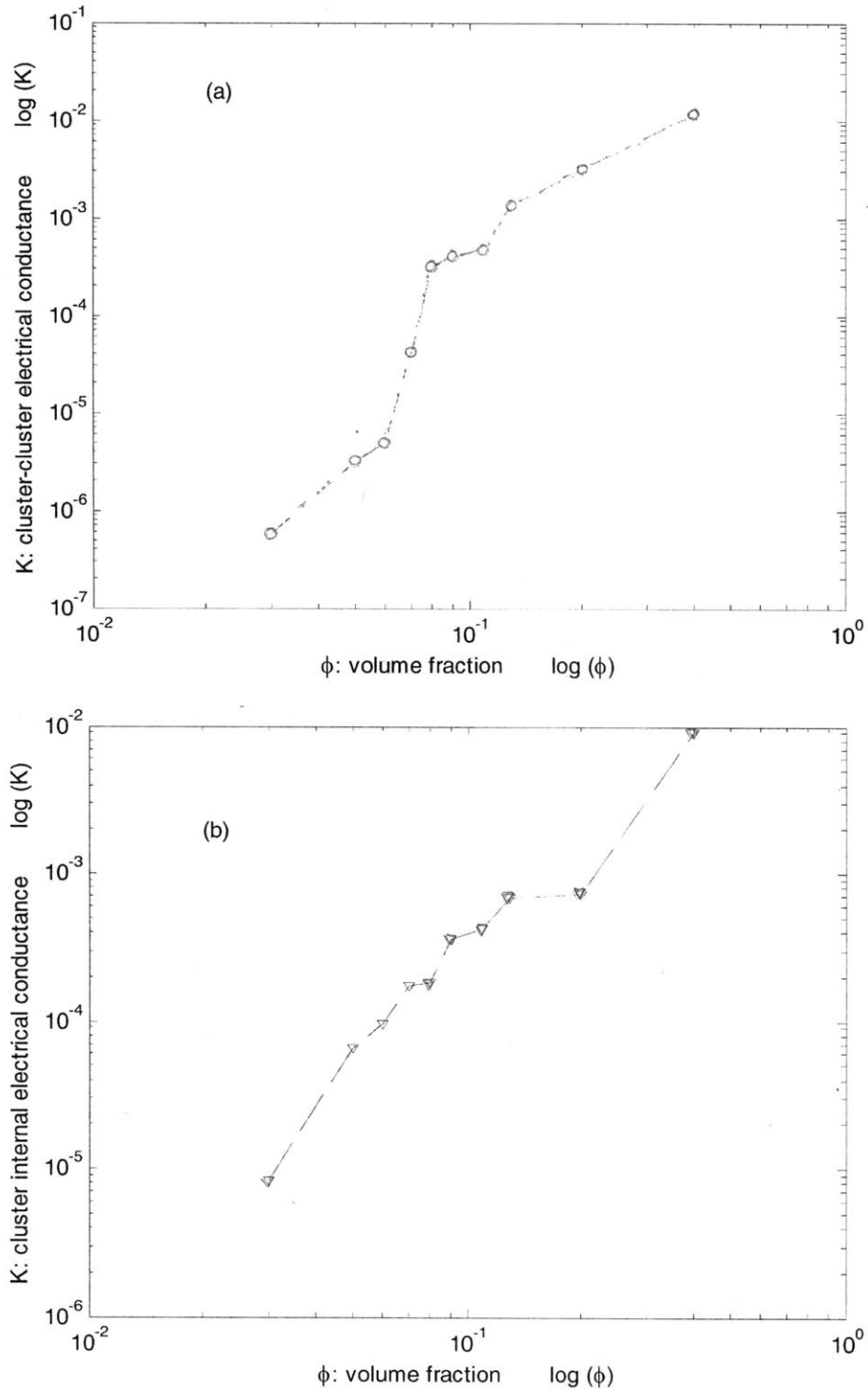


Figure 4-12: (a) cluster-cluster conductance K v.s. volume fraction ϕ in logarithm scale; (b) cluster internal conductance K v.s. volume fraction ϕ in logarithm scale.

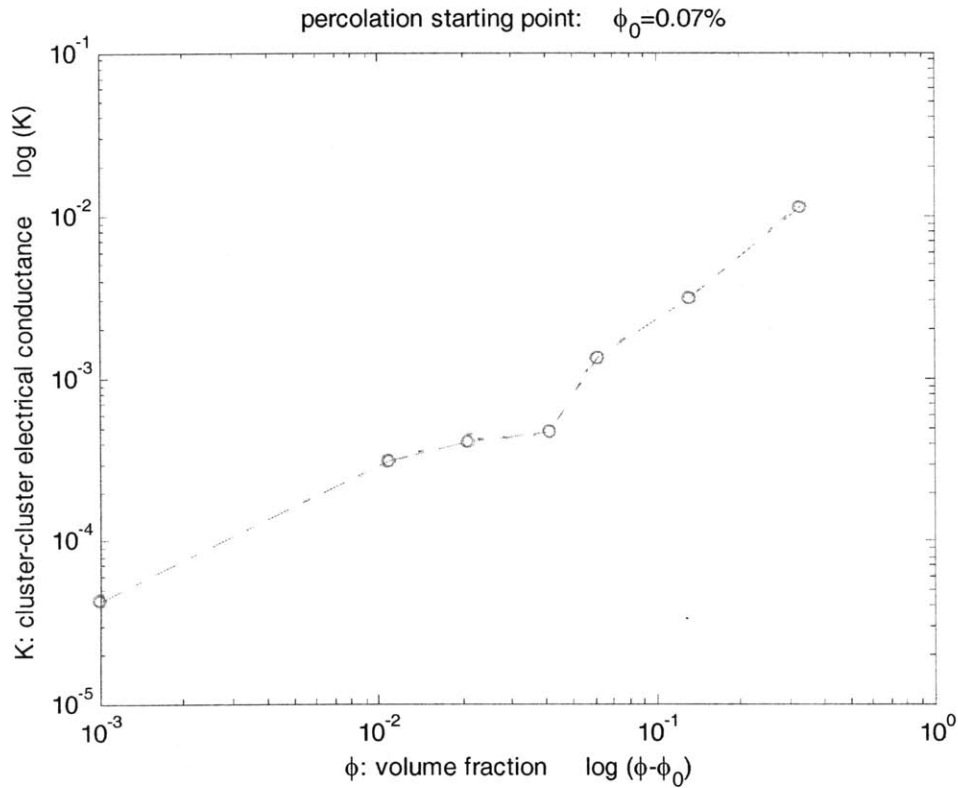


Figure 4-13: The relation between logarithm of cluster-cluster conductance K and logarithm of volume fraction ϕ in the percolation region.

As for the capacitance behavior, when the graphite volume fraction increases, the clusters within the suspension may first become more compact (to minimize the interfacial energy) and then increase the size. When the clusters become more compact, the distance between flakes within the cluster is decreased, this will cause the cluster internal capacitance increases. Then when the cluster size increases, the flakes within the cluster may become a little loosened connected, thus the distance between flakes increases slightly. This will cause the cluster internal capacitance slightly decreases. We can see this trend in Fig. 4-10 (d). Here we have assumed that the effect of distance between graphite flakes on the capacitance is more obvious than the effect of cluster size (proportional to cluster surface area), since the orientation of graphite flakes is quite random. However, the overall trend for the cluster internal capacitance should increase.

The cluster-cluster capacitance should be determined by the cluster size and the cluster-cluster separation. When the volume fraction increases, the cluster size will increase and the cluster-cluster separation will decrease. From the knowledge of plane-parallel capacitor, we should have the intuition that the cluster size is analogy to the plane area, and the cluster-cluster separation is analogy to the plane distance. Therefore, the cluster-cluster capacitance will increase as the volume fraction increases (as shown in Fig. 4-10 (c)).

Besides the above set of data, we have also prepared another set of ethylene glycol based graphite suspension samples but using shorter ultrasonic time and measured their AC impedance behavior. The cluster internal conductance & capacitance and cluster-cluster conductance & capacitance are plotted in the following (Fig. 4-14) as a function of graphite volume fraction. The samples used in Fig. 4-14 are corresponding to the blue curve in Fig. 3-13 which we redraw in Fig. 4-15.

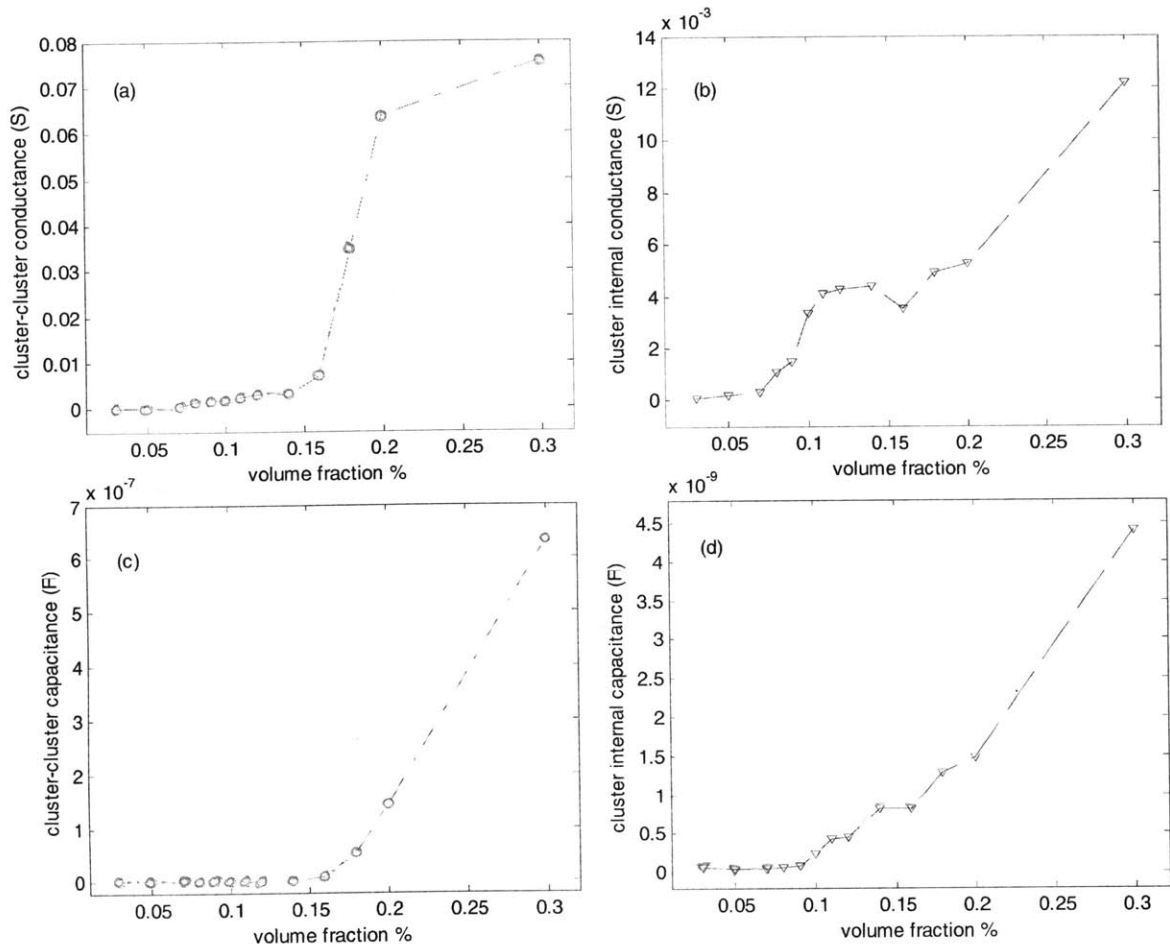


Figure 4-14: Cluster-cluster conductance & capacitance and cluster internal conductance & capacitance as a function of graphite volume fraction. Samples are prepared using shorter ultrasonic time compared with the samples of Fig. 4-10.

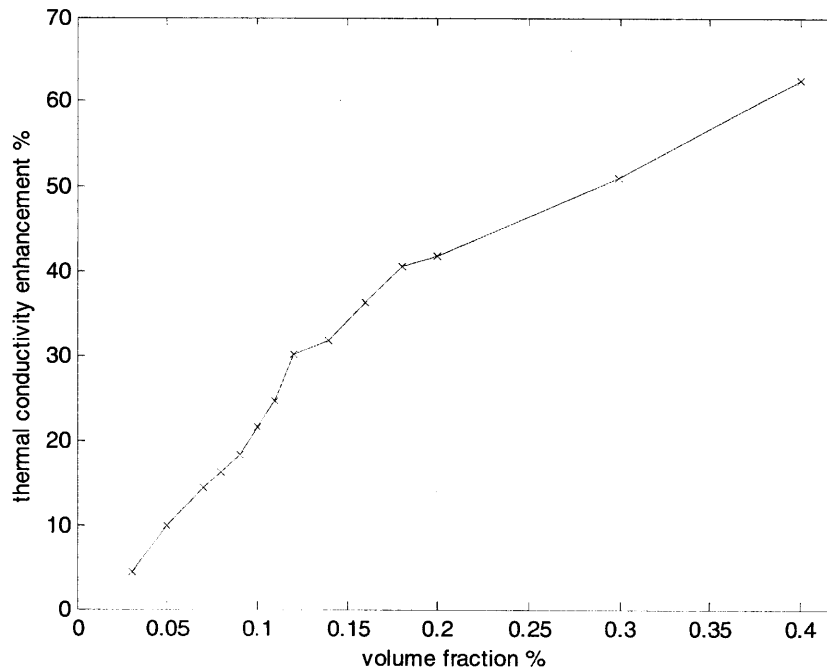


Figure 4-15: Thermal conductivity enhancement of ethylene glycol based graphite suspensions. Samples are prepared using shorter ultrasonic time compared with the samples of Fig. 4-11. The samples used in this figure are corresponding to the samples in Fig. 4-14.

When the ultrasonic time becomes shorter, the graphite flake size will become larger. Then the number of clusters will decrease for the same graphite volume fraction. Consequently the number of contacts also decreases and so does the total contact resistance. Therefore, both cluster-cluster resistance and cluster internal resistance in Fig. 4-12 (a) and (b) are smaller in the order of magnitude compared with Fig. 4-10 (a) and (b). Similar situations occur for the cluster-cluster capacitance and cluster internal capacitance, since with larger average flake size, the chances of orientation randomization are smaller, and the flakes overlaps can contribute more effectively to capacitance. However, the overall trends of these resistance and capacitance in Fig. 4-12 are similar with Fig. 4-10, although the detail shape of the figures near some volume fraction is a little different. These differences might due to the different assembly cluster structures caused by different flake size within the suspension. Understanding these differences needs to explore more experimental investigation in the future researches.

The cluster-cluster conductance versus graphite volume fraction is also plotted in the logarithm scale for the percolation region (see Fig. 4-16). Both Fig. 4-14 (a) and Fig. 4-15 show that the percolation starts at a larger volume fraction than the previous set of samples. Figure 4-15 tells the percolation point probably starts from $\phi_0 = 0.12\%$. However, Fig. 4-16 does not show linear relation. And the Fig. 4-15 also shows complicated thermal conductivity variation trend. It seems that there are two percolation points for the thermal conductivity. Understanding this complicated behavior need explore more experiments in the future.

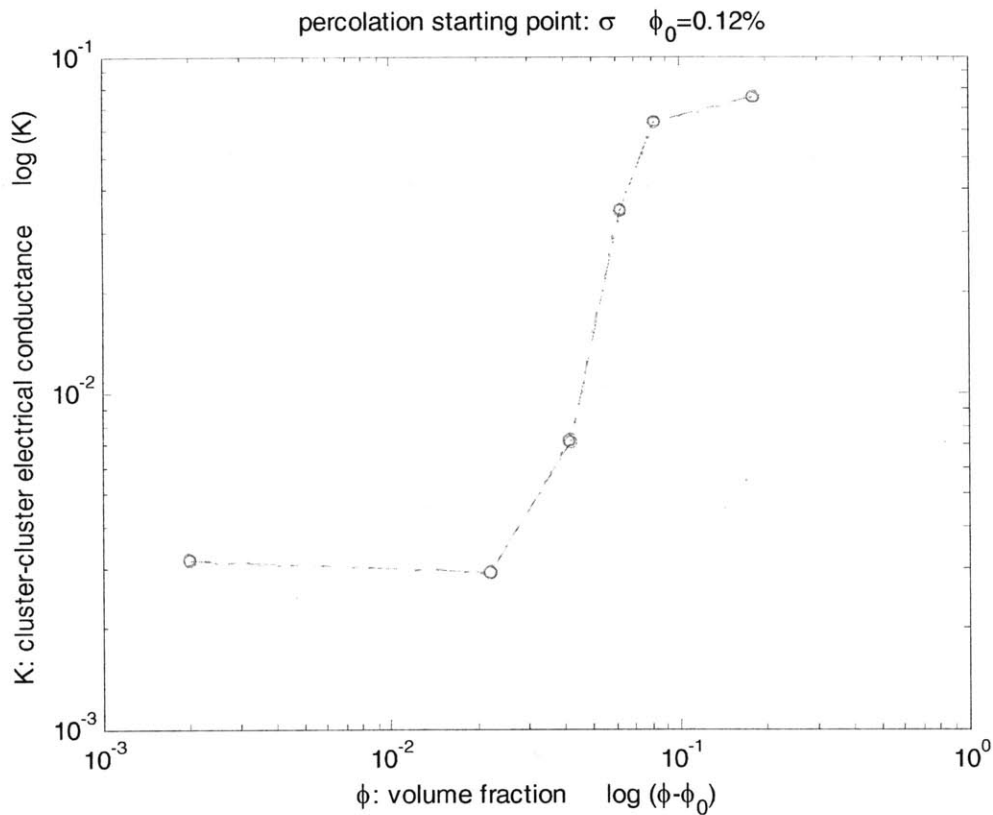


Figure 4-16: The relation between logarithm of cluster-cluster conductance K and logarithm of volume fraction ϕ in the percolation region. The samples used in this figure correspond to the samples in Fig. 4-14.

Although our experiments are mainly focused on ethylene glycol based graphite

suspensions, we also did some preliminary experiments on the AC impedance behavior of DI water based graphite suspensions. Here we are not planning to discuss the experimental results since the data is very limited so far. We want to emphasize that water molecules are polar molecules, and it has high dielectric constant, therefore the cluster internal capacitance and cluster-cluster capacitance will be much larger than that of ethylene glycol based graphite suspensions. Similar situation might occur for the cluster internal resistance and cluster-cluster resistance since the electrical conductivity of water is much higher than ethylene glycol. And because the graphite is much less hydrophilic to water than to ethylene glycol, the graphite flakes might form different self-assembly cluster structures; this might result in different resistance and capacitance behaviors for DI water based graphite suspensions from that of ethylene glycol based graphite suspensions.

It should be mentioned that in each set of data we discussed above, the ultrasonic time of samples with different volume fractions are different. Although the size of graphite flakes will not differ significantly if the ultrasonic time is not too long, we should admit that this non-identical ultrasonic time complicate data interpretation. Further experimental investigation with identical ultrasonic time will be conducted in the next step.

4.3 Summary

We employed the AC impedance spectroscopy to investigate the transport mechanisms of our graphite suspensions. The thermal and electrical transport properties of graphite suspensions are determined by the internal structures. Optical images could only give us an intuitive judgment about these internal structures. When it is combined with AC impedance spectroscopy, we obtained more detailed pictures about the internal structures and understood their evolution as the volume fraction

varies.

Chapter 5

Temperature Regulation of Electrical and Thermal Properties via Phase Transition

In addition to studying thermal conductivity of the suspensions, we also investigated the thermal and electrical conductivity contrasts of our suspensions in the liquid and the solid states. This is motivated by previous works done in our lab [39]. Gao et. al. [39] investigated the thermal conductivity enhancement of alumina nanocomposites in different phase states: the liquid state and the solid state. The motivation of their experiments was to see whether Brownian motion plays an important role in the thermal conductivity enhancement of nanocomposites. When the nanofluids are frozen, the Brownian motion effect is also significantly reduced. However, the measurement results showed that the nanocomposites in both the liquid state and the solid state have considerable thermal conductivity enhancements when crystal-forming liquid is used. And the solid-state nanocomposites have even much higher thermal conductivity enhancement when the liquid forms crystal.

The obvious different thermal conductivity enhancement between the solid-state and the liquid-state nanocomposites is an interesting result. Although it is quite well known that electrical conductivity can be tuned via temperature using the metal-insulator transition [81], temperature regulation of thermal conductivity is not that easy. If we can improve the previous work to increase the contrast of the thermal conductivity between solid state and liquid state, that may lead to practical application of our nanocomposites.

5.1 Temperature regulation of electrical and thermal properties

To conduct the experiments, we still choose to use hexadecane as the matrix. This is because the phase transition temperature of hexadecane is around 18°C , which is convenient for experimentation. For particles we choose to use graphite flakes rather than alumina, as we have shown that graphite suspensions have much higher enhancements in thermal and electrical conductivities.

We follow the same process as introduced in chapter 2 to prepare the hexadecane based graphite nanocomposites. Both electrical conductivity and thermal conductivity in the solid state and the liquid state are measured. Cyclic measurements on the electrical conductivity and the thermal conductivity were conducted to test their reversibility. Figure 5-1 shows the cyclic behavior of the electrical conductivity as the suspension going through repeated melting and freezing processes. The first freezing cycle shows largest electrical conductivity contrast because it contains more loose clusters in the liquid state. In the first remelting process, contacts between graphite flakes degrade dramatically, leading to sharp reduction in the electrical conductivity. However, many graphite flakes will be trapped in the percolation network and hence the electrical conductivity in the liquid state increases from its original synthesized state. After the first cycle, the percolation structure becomes stable, and the electrical conductivity contrast of graphite nanocomposites approaches a constant [82].

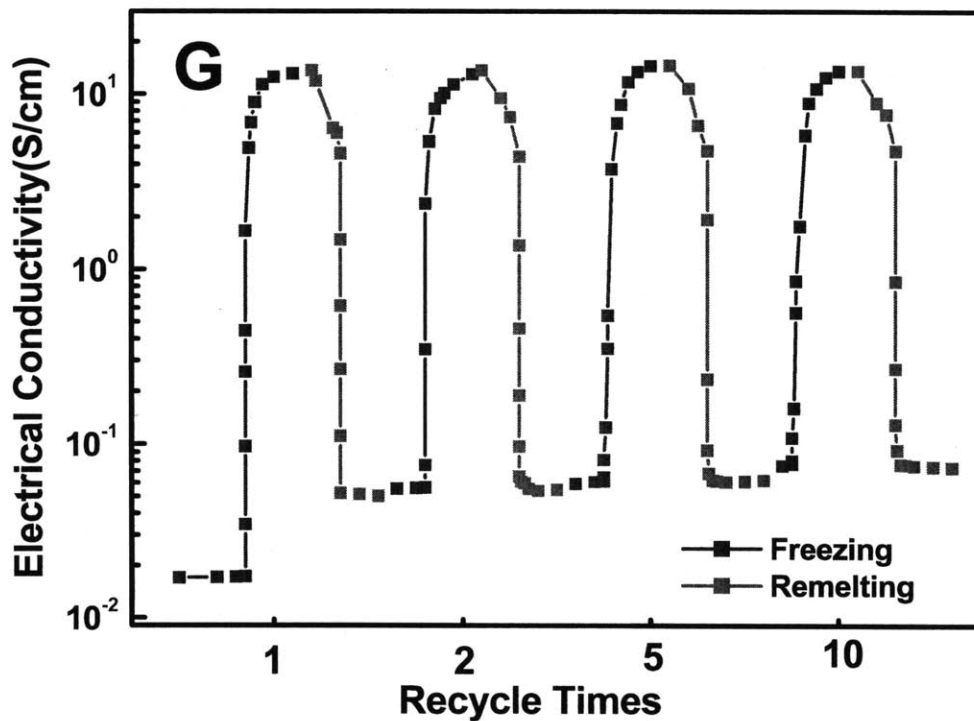


Figure 5-1: Electrical conductivity contrast after different cycles. Blue lines indicate the electrical conductivity of 0.8% hexadecane based graphite nanocomposites in the course of freezing, while red lines indicate that in the course of melting.

We also measured the thermal conductivity of the graphite suspensions in the liquid and the solid states. To get the liquid state thermal conductivity, the samples are measured at the ambient temperature. To obtain the solid state thermal conductivity, samples are measured in a small refrigerator. The measurements are still based on transient hotwire method. Cyclic measurement results on the thermal conductivity are shown in Fig. 5-2.

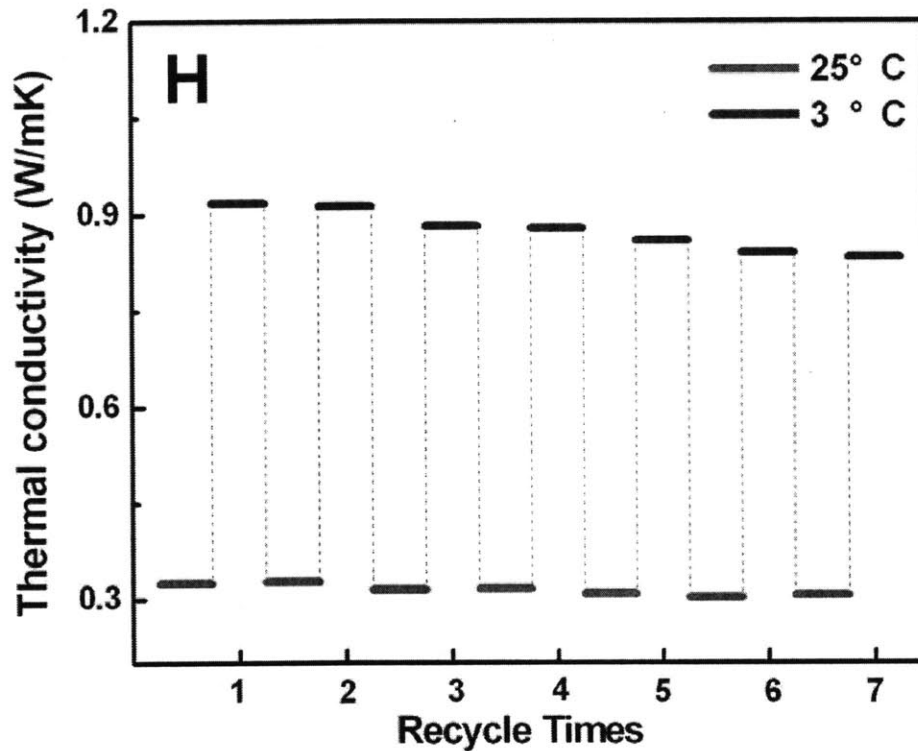


Figure 5-2: Thermal conductivity contrast after different cycles. Blue lines indicate the thermal conductivity of 0.8% hexadecane based graphite nanocomposites at 3°C during different cycles, while red lines indicate that at 25°C during different cycles.

During freezing, the graphite particles are squeezed to the grain boundaries [83-85]. The internal stress generated during freezing regulates the contacts among particles, increasing the thermal conductivity of sample. In the liquid state, the contact among graphite particles is loose and weak. Hence the interfacial thermal resistance between two flakes is high, and the total thermal conductivity of suspension is small. During the freezing of the hexadecane, needle-like structures are formed. The anisotropic growth of the hexadecane crystals generates pressure, rapidly increasing the contact area of graphite flakes and meanwhile making the contact more tightly. When the hexadecane remelts, the pressure on the graphite flakes is released and the contact area is reduced due to the elastic recovery of graphite flakes and inter-particle repulsion (see Fig. 5-3). Therefore, the stress generation during the phase change process is the key reason for the large contrast of thermal conductivity at different

states.

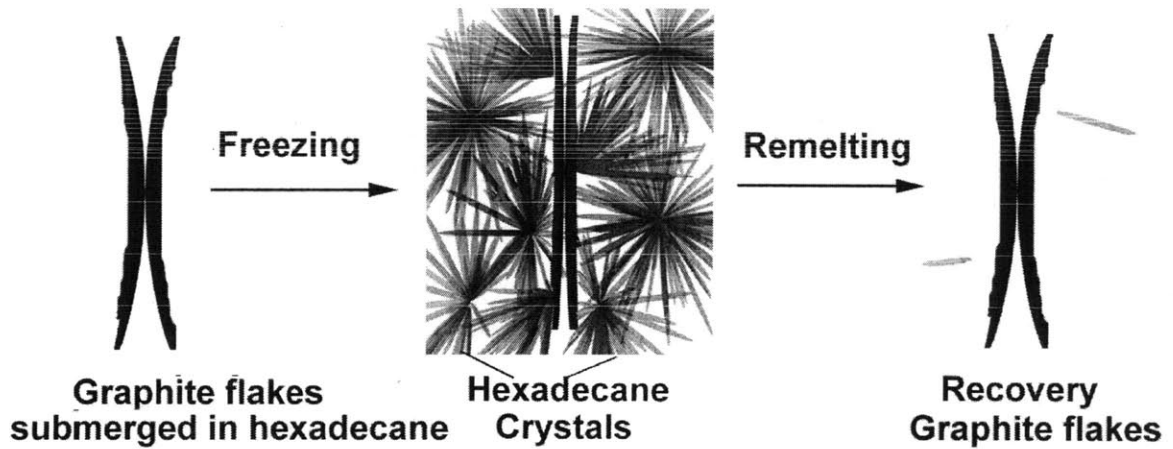


Figure 5-3: Conceptual illustration of the contact area variation between graphite flakes submerged in hexadecane in the course of hexadecane freezing and remelting. The anisotropic growth the hexadecane crystals will generate pressure on the surface of graphite flakes, which increases the contact area and reduces the flake separation. When the frozen hexadecane remelts, the pressure is released and the contact area decreases again.

5.2 Summary

The chapter showed an experimental strategy to achieve significant reversible temperature regulation of both electrical conductivity and thermal conductivity via liquid-solid phase transition. Results indicate a two orders-of-magnitude change in the electrical conductivity and a three times change in thermal conductivity around phase transition temperature 18°C can be achieved. Optimization of the suspension might result in larger thermal and electrical conductivity contrasts for potential application in the future.

Chapter 6

Conclusions and Future Work

6.1 Summary and Conclusions

In this thesis, we have introduced a new preparation method of graphite suspensions by chemical intercalation and microwave expansion, and investigated the thermal conductivity of graphite suspensions using transient hotwire method, the transport mechanisms using AC impedance spectroscopy technique, and the temperature regulation of both electrical and thermal conductivities via phase transition.

First we developed a method to prepare stable graphite suspensions in both oil and water based liquids. It is found that surface functional groups formed during intercalation and microwave expansion can be used to control hydrophilicity of graphite. While being able to maintain the hydrophilic characteristic of graphite to the ethylene glycol and organic oil, we found that proper process control makes the graphite less hydrophobic to the water, enabling the preparation of stable water based graphite suspensions.

The thermal conductivity of suspensions is one of the most important properties researchers are concerned about. Thermal conductivities of graphite suspensions based on three different fluids are investigated. Results show that the thermal conductivity can achieve very high enhancement with 1% graphite loading, exceeding the maximum values reported in the literatures. In order to achieve high thermal conductivity enhancement, certain preparation processes must be well controlled, especially the ultrasonic process. Too long ultrasonic time will reduce the thermal

conductivity of graphite suspensions significantly; too short ultrasonic time will affect the uniformity of the suspension which makes the suspensions impractical to use. We found that larger graphite flakes lead to higher thermal conductivity. Our experimental results are consistent with the picture that heat conduction via graphites is the mechanism behind the thermal conductivity enhancement.

The graphite cluster structures and the cluster distribution pattern within the suspensions will change as the volume fraction increases. Such structural changes will significantly affect the thermal conductivity. We introduced the AC impedance spectroscopy technique to study the structures of the graphite suspensions. Analyses of the electrical conductance and capacitance data tell us how the internal structures of the suspensions change as the volume fraction increases. Our experiment results confirm the percolation of graphite flakes. When combined with optical images, the AC impedance spectroscopy led to better understanding of the internal structures and their correlations to the thermal conductivity.

In addition to studying thermal conductivity of the suspension, we developed a strategy to realize reversible temperature regulation of electrical and thermal properties via phase transition. Around the phase transition temperature, two orders-of-magnitude change in electrical conductivity and three times change in thermal conductivity were achieved. These promising results may attract more research interests and lead to potential application in the future.

6.2 Future Work

Although our method can help us prepare stable graphite suspensions, the stability of water based graphite suspensions still has much room to improve. The microwave expansion method brings new functional groups to the surface of graphite flakes and thus reduces its hydrophobicity. This provides us a good idea to further improve the stability of our graphite suspensions. Understanding what kind of function groups is hydrophobic or hydrophilic and combining with surface chemistry method can give us some guidance on how to bring desirable functional groups to the surface of particles to change the material's hydrophobicity or hydrophilicity.

As we have concluded, clusters and their percolation in the suspensions are probably the key factors for the large enhancement of thermal conductivity. However, how the graphite flakes aggregate together is not quite understood so far. Understanding the interactions between two graphite flakes could help us mapping the charge distribution on the surface of graphite flake. This may be conducted by using the liquid operation mode of Atomic Force Microscope (AFM) probe technique.

Despite the progress made in this thesis, a thorough understanding of the heat transport mechanism of high thermal conductivity graphite suspensions is still very challenging. This is because the microscopic structures of graphite suspensions are extremely complex. The shape of graphite particles is flake-like, and graphite flakes overlaps with each other forming amorphous clusters within the suspension. When the volume fraction increases, the cluster size will grow up, and the clusters will eventually contact with each other forming a network-like percolation structure. Trying to understand this physical picture and construct a reasonable model to describe such system should be our future goal.

Although we have gained some insights about the transport mechanisms using AC

impedance spectroscopy technique, more impedance experiments need to be carried out to further analyze the electrical properties of graphite suspensions. More attention should be focused on suspensions with the same ultrasonic time. DI water and PAO based graphite suspensions should also be investigated intensively. More close connections between the thermal transport mechanisms and electrical transport mechanisms should be established in the future experiments.

Our experimental investigations also indicate that the thermal conductivity of hexadecane based graphite suspensions between liquid and solid states has large contrast at the phase transition temperature. This interesting phenomenon suggests new ways to develop materials with switchable properties. In the future we will carry out more experiments on different host materials whose melting points are around moderate temperature. Different host material might cause different stress changes during the phase transition process, and thus affects the interface resistance between host material and graphite flakes, and the thermal conductivity contrast at the phase change temperature. On the other hand, the thermal conductivity contrast should also depend on the properties and morphology of particles. For example, the mechanical characteristic of particles in the host material will have an effect on the stress during the phase change process. The shape of the particles can determine whether it is easy to form a percolation structure within the host materials. Varying the thickness and lateral size of the particles will increase or reduce the boundary scattering within the particles and thus affects the intrinsic thermal conductivity of particles [86]. Quite a lot of works need to be done in the next step to understand these questions.

Bibliography

- [1] A. S. Ahuja, Augmentation of Heat Transport in Laminar Flow of Polystyrene Suspension: Experiments and Results, *Journal of Applied Physics*, 1975, vol. 46, pp. 3408–3416.
- [2] C. J. Maxwell, *Electricity and Magnetism*. Oxford: Clarendon, 1873.
- [3] D. P. H. Hasselman and L. F. Johnson, Effective Thermal Conductivity of Composites with Interfacial Thermal Barrier Resistance, *Journal of Composite Materials*, vol. 21, 1987, pp. 508-515.
- [4] C.W. Sohn and M. M. Chen, Microconvective thermal conductivity in disperse two phase mixture as observed in a low velocity Couette flow experiment, *Journal of Heat Transfer, Trans. ASME*, vol, 103, 1981, pp. 47-51.
- [5] A. S. Ahuja, Augmentation of heat transport in laminar flow of polystyrene suspension, *Journal of Applied Physics*, vol. 46, 1975, pp 3408-3425.
- [6] G. Hetsroni and R. Rozenblit, Heat transfer to a liquid-solid mixture in a fume, *International Journal of Multiphase Flow*, vol. 20, 1994, pp. 671-689.
- [7] H. Masuda, A. Ebata, K. Teramae, and N. Hishinuma, Alteration of Thermal Conductivity and Viscosity of Liquid by Dispersing Ultra-Fine Particles (Dispersion of γ -Al₂O₃, SiO₂ and TiO₂ Ultra-Fine Particles), *Netsu Bussei*, vol. 4, pp. 227–233, 1993.
- [8] S. U. S. Choi, Enhancing thermal conductivity of fluids with nanoparticles. ASME FED, 1995, 231: 99-106.
- [9] S. K. Das, S. U. S. Choi, W. Yu, et al. *Nanofluids: Science and Technology*. Wiley-Interscience: Hoboken, NJ, 2008.
- [10] S. U. S. Choi, Z. G. Zhang, W. Yu, et al., Anomalous thermal conductivity enhancement in nanotube suspensions. *Appl. Phys. Lett.*, 2001, 79 (14): 2252-2254.
- [11] H. Xie, H. Lee, W. Youn, M. Choi, Nanofluids containing multiwalled carbon nanotubes and their enhanced thermal conductivities, *Journal of Applied Physics*, 94

- (8) (2003) 4967–4971.
- [12] J. A. Eastman, S. U. S. Choi, S. Li, et al., Anomalously increased effective thermal conductivities of ethylene glycol-based nanofluids containing copper nanoparticles. *Appl. Phys. Lett.*, 2001, 78 (6): 718-720.
- [13] S. Jana, A. Salehi-Khojin, W. H. Zhong, Enhancement of fluid thermal conductivity by the addition of single and hybrid nano-additives. *Thermochim. Acta.*, 2007, 462 (1-2): 45-55.
- [14] W. Yu, D. M. France, S. U. S. Choi, and J. L. Routbort, Review and Assessment of Nanofluid Technology for Transportation and Other Applications, ANL/ESD/07-9.
- [15] S. K. Das, N. Putra, P. Thiesen, et al., Temperature dependence of thermal conductivity enhancement for nanofluids. *J. Heat Trans-T. Asme*, 2003, 125 (4): 567-574.
- [16] H. Xie, J. Wang, T. Xi, Y. Liu, F. Ai, Q. Wu, Thermal conductivity enhancement of suspensions containing nanosized alumina particles, *Journal of Applied Physics*, 91 (7) (2002) 4568–4572.
- [17] X. Wang, X. Xu, S. U. S. Choi, Thermal conductivity of nanoparticle-fluid mixture. *Journal of Thermophysics and Heat Transfer*, 1999, 13 (4): 474-480.
- [18] S. Lee, S. U. S. Choi, S. Li, J. A. Eastman, Measuring thermal conductivity of fluids containing oxide nanoparticles, *Journal of Heat Transfer*, 121 (1999) 280–289.
- [19] D. Wen, Y. Ding, Effective thermal conductivity of aqueous suspensions of carbon nanotubes (carbon nanotube nanofluids), *Journal of Thermophysics and Heat Transfer*, 18 (4) (2004) 481–485.
- [20] T. K. Hong, H. S. Yang, C. J. Choi, Study of the enhanced thermal conductivity of Fe nanofluids. *J. Appl. Phys.*, 2005, 97 (6): 064311-4.
- [21] K. S. Hong, T. K. Hong, H. S. Yang, Thermal conductivity of Fe nanofluids depending on the cluster size of nanoparticles. *Appl. Phys. Lett.*, 2006, 88 (3): 031901-3.
- [22] S. A. Putnam, D. G. Cahill, P. V. Braun, et al. Thermal conductivity of nanoparticle suspensions. *J. Appl. Phys.*, 2006, 99 (8): 084308-6.
- [23] H. E. Patel, S. K. Das, T. Sundararagan, A. S. Nair, B. Geoge, T. Pradeep,

Thermal conductivities of naked and monolayer protected metal nanoparticle based nanofluids: Manifestation of anomalous enhancement and chemical effects, *Applied Physics Letters* 83 (2003) 2931–2933.

[24] <http://mit.edu/nse/nanofluids/benchmark/index.html>

[25] J. Buongiorno, N. P. Venerus, N. Prabhat, et al. A Benchmark Study on the Thermal Conductivity of Nanofluids. *Journal of Applied Physics*, 2009, in press.

[26] D. H. Kumar, H. E. Patel, V. R. R. Kumar, T. Sundararajan, T. Pradeep, and S. K. Das. Model for Heat Conduction in Nanofluids. *Phys. Rev. Lett.*, 2004, vol. 93, p. 144301.

[27] Y. Xuan, Q. Li, and W. Hu, Aggregation Structure and Thermal Conductivity of Nanofluids, *AIChE J.*, 2004, vol. 49, pp. 1038–1043.

[28] W. Yu, and S. U. S. Choi. The Role of Interfacial Layers in the Enhanced Thermal Conductivity of Nanofluids: A Renovated Maxwell Model. *J. Nanopart. Res.*, 2003, vol. 5, pp. 167–171.

[29] Q. Z. Xue, Model for Effective Thermal Conductivity of Nanofluids, *Phys. Lett. A*, 2003, vol. 307, pp. 313–317.

[30] H. Xie, M. Fujii, and X. Zhang. Effect of Interfacial Nanolayer on the Effective Thermal Conductivity of Nanoparticle-Fluid Mixture. *Int. J. Heat Mass Transfer*, 2005, vol. 48, pp. 2926–2932.

[31] Q. Xue, and W.-M. Xu. A Model of Thermal Conductivity of Nanofluids With Interfacial Shells. *Mater. Chem. Phys.*, 2005, vol. 90, pp. 298–301.

[32] P. Tillman, and J. M. Hill. Determination of Nanolayer Thickness for a Nanofluid. *Int. Commun. Heat Mass Transfer*, 2007, vol. 34, pp. 399–407.

[33] J. Avsec, and M. Oblak. The Calculation of Thermal Conductivity, Viscosity and Thermodynamic Properties for Nanofluids on the Basis of Statistical Nanomechanics. *Int. J. Heat Mass Transfer*, 2007, vol. 50, pp. 4331–4341.

[34] P. Keblinski, S. R. Phillpot, S. U. S. Choi, and J. A. Eastman, Mechanism of Heat Flow in Suspension of Nano-Sized Particles (Nanofluids), *International Journal of Heat and Mass Transfer*, 2002, vol. 45, pp. 855–863.

[35] W. Evans, R. Prasher, J. Fish, P. Meakin, P. E. Phelan, and P. Keblinski, Effect

of Aggregation and Interfacial Thermal Resistance on Thermal Conductivity of Nanocomposites and Colloidal Nanofluids, *International Journal of Heat and Mass Transfer*, 2008, vol. 51, pp. 1431–1438.

[36] J. Avsec, The Combined Analysis of Phonon and Electron Heat Transfer Mechanism on Thermal Conductivity for Nanofluids, *International Journal of Heat and Mass Transfer*, 2008, vol. 51, pp. 4589–4598.

[37] J. Koo, and C. Kleinstreuer, Impact Analysis of Nanoparticle Motion Mechanisms on the Thermal Conductivity of Nanofluids, *International Communications in Heat and Mass Transfer*, 2005, vol. 32, pp. 1111–1118.

[38] J. Buongiorno, Convective Transport in Nanofluids, *Journal of Heat Transfer*, 2006, vol. 128, pp. 241–250.

[39] J. W. Gao, R. T. Zheng, H. Ohtani, D. S. Zhu, G. Chen, Experimental Investigation of Heat Conduction Mechanisms in Nanofluids: Clue on Clustering, *Nano Letter*, 2009, 9 (12): 4128-4132.

[40] X. Q. Wang, A. S. Mujumdar, Heat transfer characteristics of nanofluids: a review, *International Journal of Thermal Sciences*, vol. 46, 2007, pp. 1–19.

[41] J. A. Eastman, U. S. Choi, S. Li, L. J. Thompson, S. Lee, Enhanced thermal conductivity through the development of nanofluids, *Materials Research Society Symposium – Proceedings*, vol. 457, Materials Research Society, Pittsburgh, PA, USA, Boston, MA, USA, 1997, pp. 3–11.

[42] H. Akoh, Y. Tsukasaki, S. Yatsuya, A. Tasaki, Magnetic properties of ferromagnetic ultrafine particles prepared by vacuum evaporation on running oil substrate, *Journal of Crystal Growth* 45 (1978) 495–500.

[43] M. Wagener, B.S. Murty, B. Gunther, Preparation of metal nanosuspensions by high-pressure DC-sputtering on running liquids, in: S. Komarnenl, J.C. Parker, H.J. Wollenberger (Eds.), *Nanocrystalline and Nanocomposite Materials II*, vol. 457, Materials Research Society, Pittsburgh, PA, 1997, pp. 149–154.

[44]http://www.substech.com/dokuwiki/doku.php?id=stabilization_of_colloids&DokuWiki=9254b26f6969bc8bf8da63e01bf2b4f7

- [45] B. Derjaguin, L. Landau, Theory of the stability of strongly charged lyophobic sols and of the adhesion of strongly charged particles in solutions of electrolytes. *Acta Physico Chemica URSS*, 1941, vol. 14, pp. 633.
- [46] E. J. W. Verwey, J. Th. G. Overbeek, (1948), *Theory of the stability of lyophobic colloids*, Amsterdam: Elsevier, 1948.
- [47] K. D. Kihm, *ANNUAL REPORT: Fundamentals of Energy Transport in Nanofluids*, 2004.
- [48] M. Dresselhaus, G. Dresselhaus, and K. Sugihara. *Graphite fibers and filaments*. Springer-Verlag, 1988.
- [49] K. Kalaitzidou, H. Fukushima, and L. T. Drzal, A new compounding method for exfoliated graphite-polypropylene nanocomposites with enhanced flexural properties and lower percolation threshold, *Compos Sci Technol* 2007, vol. 67, pp. 2045-2051.
- [50] K. Kalaitzidou, H. Fukushima, and L. T. Drzal, Mechanical properties and morphological characterization of exfoliated graphite-polypropylene nanocomposites, *Compos Part a-Appl S* 2007, vol. 38, pp. 1675-1682.
- [51] S. Stankovich, et al. Graphene-based composite materials. *Nature*, 2006, vol. 442, pp. 82-286.
- [52] A. Yasmin, J. J. Luo, and I. M. Daniel, Processing of expanded graphite reinforced polymer nanocomposites. *Compos Sci Technol*, 2006, vol. 66, pp. 1182-1189.
- [53] R. T. Zheng, J. W. Gao, J. J. Wang, and G. Chen, Reversible temperature regulation of electrical and thermal conductivity via liquid-solid phase transition, submitted for publication.
- [54] M. Dresselhaus, G. Dresselhaus, Intercalation compounds of graphite, *Advances in Physics*, 2002, vol. 51, No. 1, pp. 1-186.
- [55] C. Ruggiero, M. Mantelli, and A. Curtis, The effect of DLVO, hydrophilic and hydrophobic energies on the aggregation of cells in solution. *European Cells and Materials*, vol. 4, suppl. 2, 2002, pp. 115-117.
- [56] Zeta Potential - An Introduction in 30 Minutes, *Zetasizer Nano series technical note*.

- [57] http://www.bic.com/products/zeta_potential/p_ZP_ZetaPALS.html
- [58] D. C. Henry, *Proc. Roy. Soc. Ser. A*, London, 133:106.
- [59] C. H. Li, W. Williams, J. Buongiorno, et al., Transient and Steady-State Experimental Comparison Study of Effective Thermal Conductivity of Al₂O₃/Water Nanofluids, *J. Heat Transfer*, 2008, 130 (4): 042407-7.
- [60] Y. Nagasakat, A. Nagashima, *J. Phys. E*, 1981, 14: 1435-1440.
- [61] A. J. Schmidt, M. Chiesa, D. H. Torchinsky, et al., Thermal conductivity of nanoparticle suspensions in insulating media measured with a transient optical grating and a hotwire, *J. Appl. Phys.*, 2008, 103 (8): 083529-5.
- [62] B. Yang, Z. H. Han, Temperature-dependent thermal conductivity of nanorod based nanofluids, *Appl. Phys. Lett.*, 2006, 89 (8): 083111-3.
- [63] Z. Wang, D. Tang, S. Liu, et al., Thermal-Conductivity and Thermal-Diffusivity Measurements of Nanofluids by 3ω Method and Mechanism Analysis of Heat Transport, *Int. J. Thermophys.*, 2007, 28 (4): 1255-1268.
- [64] R. Rusconi, E. Rodari, R. Piazza, Optical measurements of the thermal properties of nanofluids, *Appl. Phys. Lett.*, 2006, 89 (26): 261916-3.
- [65] A. J. Schmidt, M. Chiesa, D. H. Torchinsky, et al. Thermal conductivity of nanoparticle suspensions in insulating media measured with a transient optical grating and a hotwire. *J. Appl. Phys.* 2008, 103, 083529.
- [66] Y. Ding, H. Alias, D. Wen, et al., Heat transfer of aqueous suspensions of carbon nanotubes (CNT nanofluids), *Int. J. Heat and Mass Transfer*, 2006, 49 (1-2): 240-250.
- [67] H. Hong, B. Wright, J. Wensel, et al., Enhanced thermal conductivity by the magnetic field in heat transfer nanofluids containing carbon nanotube, *Synth. Met.*, 2007, 157 (10-12): 437-440.
- [68] D. Wen, Y. Ding, Effective thermal conductivity of aqueous suspensions of carbon nanotubes (carbon nanotube nanofluids), *J. Thermophys. Heat Transfer*, 2004, 18 (4): 481-485.
- [69] J. J. Ma, *Thermal Conductivity of Fluids Containing Suspension of Nanometer-Sized Particles*, Master Thesis, Massachusetts Institute of Technology, 2006.

- [70] J. W. Haarman, A contribution to the theory of the transient hot-wire method. *Physica*, 1971, vol. 52, pp. 605-619.
- [71] J. W. Gao, *Experimental and Theoretical Investigation of High Thermal Conductivity Micro/Nano- Fluids*, PhD Thesis, South China University of Technology & Massachusetts Institute of Technology, 2010.
- [72] S. Shaikh, K. Lafdi, R. Ponnappan, Thermal conductivity improvement in carbon nanoparticle doped PAO oil: An experimental study. *J. Appl. Phys.*, 2007, 101 (6): 064302-7.
- [73] H. Zhu, C. Zhang, Y. Tang, et al., Preparation and thermal conductivity of suspensions of graphite nanoparticles, *Carbon*, 2007, 45 (1): 226-228.
- [74] M. J. Assael, C. F. Chen, I. Metaxa, et al., Thermal Conductivity of Suspensions of Carbon Nanotubes in Water, *Int. J. Thermophys.*, 2004, 25 (4): 971-985.
- [75] H. Xie, L. Chen, Adjustable thermal conductivity in carbon nanotube nanofluids, *Phys. Lett. A*, 2009, 373 (21): 1861-1864.
- [76] M. J. Assael, C. F. Chen, I. Metaxa, et al., Thermal Conductivity of Suspensions of Carbon Nanotubes in Water, *Int. J. Thermophys.*, 2004, 25 (4): 971-985.
- [77] C. H. Li, G. P. Peterson, Experimental investigation of temperature and volume fraction variations on the effective thermal conductivity of nanoparticle suspensions (nanofluids), *J. Appl. Phys.*, 2006, 99 (8): 084314-8.
- [78] A. Lasia, *Electrochemical Impedance Spectroscopy and its Applications*, Kluwer Academic/Plenum Publishers, New York, 1999, vol. 32, pp. 143-248.
- [79] E. Barsoukov, J. R. Macdonald, *Impedance Spectroscopy: Theory, Experiment, and Applications*, Wiley-Interscience, 2005.
- [80] Basics of Electrochemical Impedance Spectroscopy, *Gamry Instruments Application Notes*.
- [81] R. G. Moore, et al., A surface--tailored, purely electronic, mott metal-to-insulator transition, *Science*, 2007, vol. 318, pp. 615-619.
- [82] R. T. Zheng, J. W. Gao, G. Chen, *Thermal and/or Electrical Conductivity Controls in Suspensions*, Patent pending.
- [83] S. Deville, E. Saiz, R. K. Nalla, A. P. Tomsia, Freezing as a Path to Build

Complex Composites, *Science* 311, 515-518 (2006).

[84] K. M. Golden, S. F. Ackley, V. I. Lytle, The percolation phase transition in sea ice. *Science* 1998, vol, 282, pp. 2238-2241.

[85] D. Porter, K. Easterling, *Phase transformations in metals and alloys*. (CRC, 1992).

[86] G. Chen, *Thermally Regulation of Heat Transfer Processes*, Research Proposal (submitted).